Science of the Total Environment 904 (2023) 166815

Contents lists available at ScienceDirect

Science of the Total Environment

journal homepage: www.elsevier.com/locate/scitotenv

Evaluation of flash drought under the impact of heat wave events in southwestern Germany

Menghao Wang [a,b,c], Lucas Menzel [d,*], Shanhu Jiang [a,b,c,**], Liliang Ren [a,b,c], Chong-Yu Xu [e], Hao Cui [c]

[a] The National Key Laboratory of Water Disaster Prevention, Hohai University, Nanjing 210098, China
[b] Cooperative Innovation Center for Water Safety and Hydro-Science, Hohai University, Nanjing 210098, China
[c] College of Hydrology and Water Resources, Hohai University, Nanjing 210098, China
[d] Department of Geography, Professorship in Hydrology and Climatology, Heidelberg University, Heidelberg D-69120, Germany
[e] Department of Geosciences, University of Oslo, Oslo, Norway

HIGHLIGHTS

- A physically based hydrological model was evaluated and then applied for flash drought studies.
- Frequency of flash droughts and heat waves in southwestern Germany showed a significant ($p < 0.05$) upward trend.
- Flash droughts under the impact of heat waves are often shorter in duration but faster in onset speed.

GRAPHICAL ABSTRACT

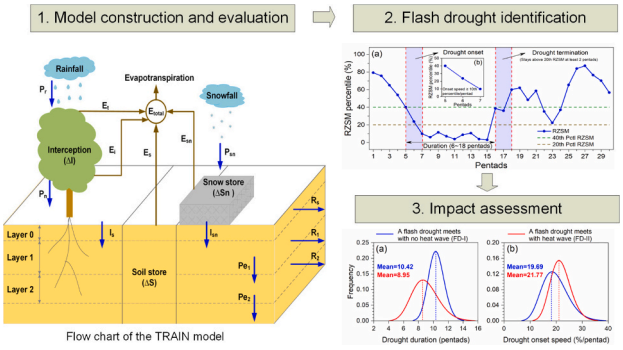

Flow chart of the TRAIN model

ARTICLE INFO

Editor: Fernando A.L. Pacheco

Keywords:
Flash drought
Heat waves
Root zone soil moisture
Evapotranspiration
TRAIN model

ABSTRACT

Flash droughts are a recently recognised type of extreme drought defined by the rapid onset and strong intensification of drought conditions. Our understanding of flash drought processes under the influence of heat waves needs to be improved in the context of global warming. Here, we applied a physically based hydrological model, i.e., TRAnspiration and INterception (TRAIN) model to simulate root zone soil moisture (RZSM) and evapotranspiration (ET) with daily time steps and at a 1 × 1 km resolution to identify and assess flash droughts. Two states, Baden-Württemberg (BW) and Rhineland-Palatinate (RP), located in southwestern Germany, were selected as the study areas. Three datasets, the Global Land Evaporation Amsterdam Model (GLEAM) dataset, ERA5-Land (land component of the fifth generation of European ReAnalysis) dataset, and SMAP-L4 (Soil Moisture Active Passive Level-4) dataset, were selected to evaluate the TRAIN simulated RZSM and ET from 1961 to 2016. The results show that the simulated RZSM had the highest correlation with the ERA5-Land products, followed by SMAP-L4 and GLEAM, with regional average correlation coefficients (CC) of 0.765, 0.762, and 0.746, respectively. The CC of the TRAIN simulated ET with ERA5-Land and GLEAM ET were 0.828 and 0.803,

* Corresponding author.
** Correspondence to: S. Jiang, The National Key Laboratory of Water Disaster Prevention, Hohai University, Nanjing 210098, China.
E-mail addresses: lucas.menzel@uni-heidelberg.de (L. Menzel), hik0216@hhu.edu.cn (S. Jiang).

https://doi.org/10.1016/j.scitotenv.2023.166815
Received 8 July 2023; Received in revised form 24 August 2023; Accepted 2 September 2023
Available online 4 September 2023

respectively. The results of the trend analyses showed a significant increase ($p < 0.05$) in the number of flash droughts and heat waves in both the BW and RP states. A comparative analysis revealed that the mean duration and onset speed of flash droughts in BW (RP) without heat waves were 10.42 (10.67) pentads and 19.69th percentile/pentad (17.16th percentile/pentad), respectively, while associated with heat waves they were 8.95 (9.53) pentads and 21.77th percentile/pentad (19.91th percentile/pentad), respectively. This indicates that flash droughts under the influence of heat waves are generally shorter in duration but faster in occurrence. The findings of this study have important implications for flash drought assessment, monitoring, and mitigation under the impact of heat waves.

1. Introduction

Drought is a complex and multidimensional disaster that threatens water security (Van Loon et al., 2016; Jiang et al., 2019, 2022; Wang et al., 2020, 2021; Tijdeman and Menzel, 2021). Conventional droughts develop slowly and span several months to years (Mishra and Singh, 2010; Van Loon and Van Lanen, 2013; Huang et al., 2017; AghaKouchak et al., 2021). However, flash drought, a new term of drought proposed by Svoboda et al. (2002), can rapidly develop into a severe drought condition from a non-drought state, with a rapid onset speed of several days or weeks (Otkin et al., 2018; Yuan et al., 2019; Liu et al., 2020a, 2020b; Zhang et al., 2022). Recently, a number of high-impact flash drought events have been reported worldwide, such as the summer 2012 mega drought in the Midwestern Plains of the United States (Otkin et al., 2016), flash droughts in the middle and lower Yangtze River in China in 2013 (Yuan et al., 2015), flash droughts in southern Africa from 2015 to 2016 (Yuan et al., 2020), and flash droughts in eastern Australia from 2017 to 2018 (Nguyen et al., 2019). Therefore, it is important to understand the complex causes and processes involved in the occurrence of flash droughts, particularly in the context of changing environmental conditions.

Svoboda et al. (2002) coined the term "flash drought" to draw attention to the unusually rapid intensification of some drought events and then better separate these events from slowly evolving traditional droughts (Otkin et al., 2018). According to the relevant literature, the definition of flash drought has experienced three main stages (Yuan et al., 2020). In the first stage, the occurrence of a flash drought was determined using a composite indicator based on multifactorial variables, such as air temperature, precipitation, evapotranspiration (ET), and soil moisture (SM). Typically, Mo and Lettenmaier (2015, 2016) adopted different combinations of thresholds for the above variables to define two types of flash droughts: the precipitation deficit flash drought (PDFD) and the heat waves flash drought (HWFD). In the second stage, Otkin et al. (2018) argued that the definition of flash drought should inherently account for both its rapid intensification (i.e., the flash) and the actual condition of moisture limitation (i.e., the drought). As the proposed definition focuses on the intensification rate, it is necessary to depict changes in a specific variable (e.g., ET and SM) over a period of time to identify a flash drought event, which completes the transformation in flash drought identification from a multi-factor composite indicator to a single-factor velocity indicator. Unfortunately, this definition either does not provide a clear duration limit for the drought development process to separate it from slowly developing drought events or does not consider the termination phase of a flash drought, failing to provide a complete drought persistence attribute to flash drought events (Yuan et al., 2020). Currently, a flash drought is defined as a type of drought with rapid intensification and a complete development and termination process on sub-seasonal timescales (Yuan et al., 2019). For example, Shah et al. (2022) stated that a flash drought in Europe starts when the soil moisture above the 40th percentile falls below the 20th percentile in less than three following pentads (1 pentad = 5 days), with a mean decline rate of no less than the 10th percentile per pentad (i.e., a decrease of 10 percentile of soil moisture during one pentad). A flash drought terminates when the soil moisture rises above the 20th percentile threshold and remains above this threshold for at least two pentads. The duration of a flash drought event is considered to be between 6 and 18 pentads. In this study, we applied this definition to identify flash droughts. A comprehensive overview of definition of flash drought can be found in Lima Alencar and Paton (2022).

Soil moisture is a commonly used variable for drought identification because of its important role in controlling the exchange of water and heat in the process of land-atmosphere feedback (AghaKouchak et al., 2015; Zhang et al., 2022). Furthermore, the root zone soil moisture (RZSM), closely related to plant growth, is recognised as an effective indicator for monitoring and identifying flash droughts (Otkin et al., 2018). Currently, there are three ways to obtain RZSM data: in situ observations, remote sensing techniques, and model simulations. Firstly, in situ observations, which provide soil moisture at different depths through ground-based instruments, are considered the most direct and accurate method to measure soil moisture (Babaeian et al., 2019). However, the spatial heterogeneity of soil moisture and the lack of dense soil moisture networks at regional or global scales make point-based observations less representative, which in turn limits their application in drought research (Peng et al., 2017; Liu et al., 2020a). Remote sensing (RS) techniques provide powerful tools for the characterisation and monitoring of near-surface soil properties (Babaeian et al., 2019). Numerous studies have provided surface and near-surface soil moisture estimates at various spatial scales (Li and Rodell, 2013; Zhang et al., 2014; Chen et al., 2018), such as the Soil Moisture and Ocean Salinity (SMOS) and Soil Moisture Active Passive (SMAP) datasets. However, owing to the limited measurement depth of microwaves, a combination of data assimilation techniques and hydrological models is usually required to invert the RZSM based on near-surface remote sensing-observed SM, which introduces some uncertainties and errors (Draper et al., 2012; Dumedah et al., 2015). In addition to point and remotely sensed observations, several re-analysis products based on model simulations provide an alternative way to obtain continuous RZSM (Yuan et al., 2015), such as datasets from the Global Land Data Assimilation System (GLDAS), the Global Land Evaporation Amsterdam Model (GLEAM) product, components of the fifth generation of the European ReAnalysis (ERA5-Land), and the North American Land Data Assimilation System (NLDAS). These datasets are important complements to in situ and remotely sensed observations (Liu et al., 2020b). However, some limitations are found in such databases, such as data gaps (Almendra-Martín et al., 2021), limited data length and spatial resolution (Liu et al., 2020b), or breaks due to its merging algorithm (Preimesberger et al., 2021). In contrast, land surface modelling ensure the completeness of separate variables at the global and regional scale, such as RZSM and ET, to enhance research in drought studies (Almendra-Martín et al., 2022). More importantly, these models feature physically based formulations to describe RZSM and ET, and they include high-resolution hydro-meteorological data and their interpolation (often combining ground observations with reanalysis and remote sensing) to generate highly spatial and temporal RZSM and ET simulations. Therefore, in this study, we applied the TRAnspiration and INterception (TRAIN) model (Menzel, 1996, 1997) to generate daily RZSM and ET at a 1 × 1 km spatial resolution.

In addition to flash droughts, heat waves, a type of extreme disaster caused by abnormally high air temperatures, have also attracted global concern owing to their rapid pace of development and devastating

effects (Perkins, 2015). More importantly, several studies have stated that global warming causes an increase in the frequency of heat waves and flash droughts (Hao et al., 2022; Qing et al., 2022; Mukherjee et al., 2023), as well as an increase in the probability of the coincidence of these two extreme events in some hotspot areas, including Europe (Shah et al., 2022), Asia (Wang and Yuan, 2022; Zhang et al., 2023a), and American (Edris et al., 2023). For example, a heat wave accompanied by a severe soil moisture deficit in Russia in 2010 killed approximately 54,000 individuals, reduced crop yields by approximately 25 %, and led to a total economic loss of ~US$15 billion (Peters et al., 2010). In the summer of 2018, Central Europe experienced a severe heat wave caused by a combination of prolonged precipitation, soil moisture deficits, and abnormally high temperatures, beginning in May 2018. Based on satellite observations, biomass accumulation has been found to decline by 15 %–25 %, even exceeding 25 % locally (Toreti et al., 2019). Such combined extremes (e.g., droughts and heat waves) may lead to adverse impacts on water supply, crop yield, and livestock mortality, which can be higher than the sum of their individual components (Ward et al., 2022). However, researches on the impact of heat waves on flash droughts is limited recently. Thus, the scientific question that this study focus on is how the flash drought characteristics (e.g., drought duration and onset speed) and their associated hydro-meteorological variables change under the influence of heat waves. Meanwhile, the main hypothesis of this study is that flash drought events with and without heat wave encounters are independent of each other and can be compared.

We selected the southwestern German states of Baden-Württemberg (BW) and Rhineland-Palatinate (RP) as study regions. For the simulation of the daily RZSM and ET at a 1 × 1 km spatial resolution and the subsequent identification of flash droughts, we applied the TRAIN model (Menzel, 1996, 1997), which was successfully adopted under the given climatic conditions. The objectives of this study were to (1) evaluate the TRAIN simulated RZSM and ET from 1961 to 2016 by comparing them with three datasets, i.e., GLEAM, ERA5-Land, and SMAP-L4; (2) identify heat waves and flash drought events based on the daily maximum temperature and TRAIN simulated RZSM, and analyse the spatial and temporal distributions of flash droughts, heat waves, and the coincidence of these two events; and (3) divide the flash drought events into two types: flash droughts that meet with no heat waves and those that occur simultaneously, and then compare drought characteristics of the two types of flash droughts (e.g., duration and onset speed) and changes in the hydro-meteorological variables (e.g., precipitation, ET, and temperature) associated with the flash drought processes to reveal how heat waves alter flash drought processes. The novelty of our study lies in the combined consideration of the two types of flash droughts and how heat waves modify these natural events. The results of this study can advance our understanding of the occurrence and dynamics of flash droughts.

2. Study area and data

2.1. Study area

In this study, Rhineland-Palatinate (19,853 km^2) (RP) and Baden-Württemberg (35,751 km^2) (BW), two of the 16 states in the Federal Republic of Germany (Fig. 1), were selected as the study area. This region forms southwest Germany and has an altitude between 38 and 1494 m.a.s.l. It belongs to a temperate humid climate zone, which has

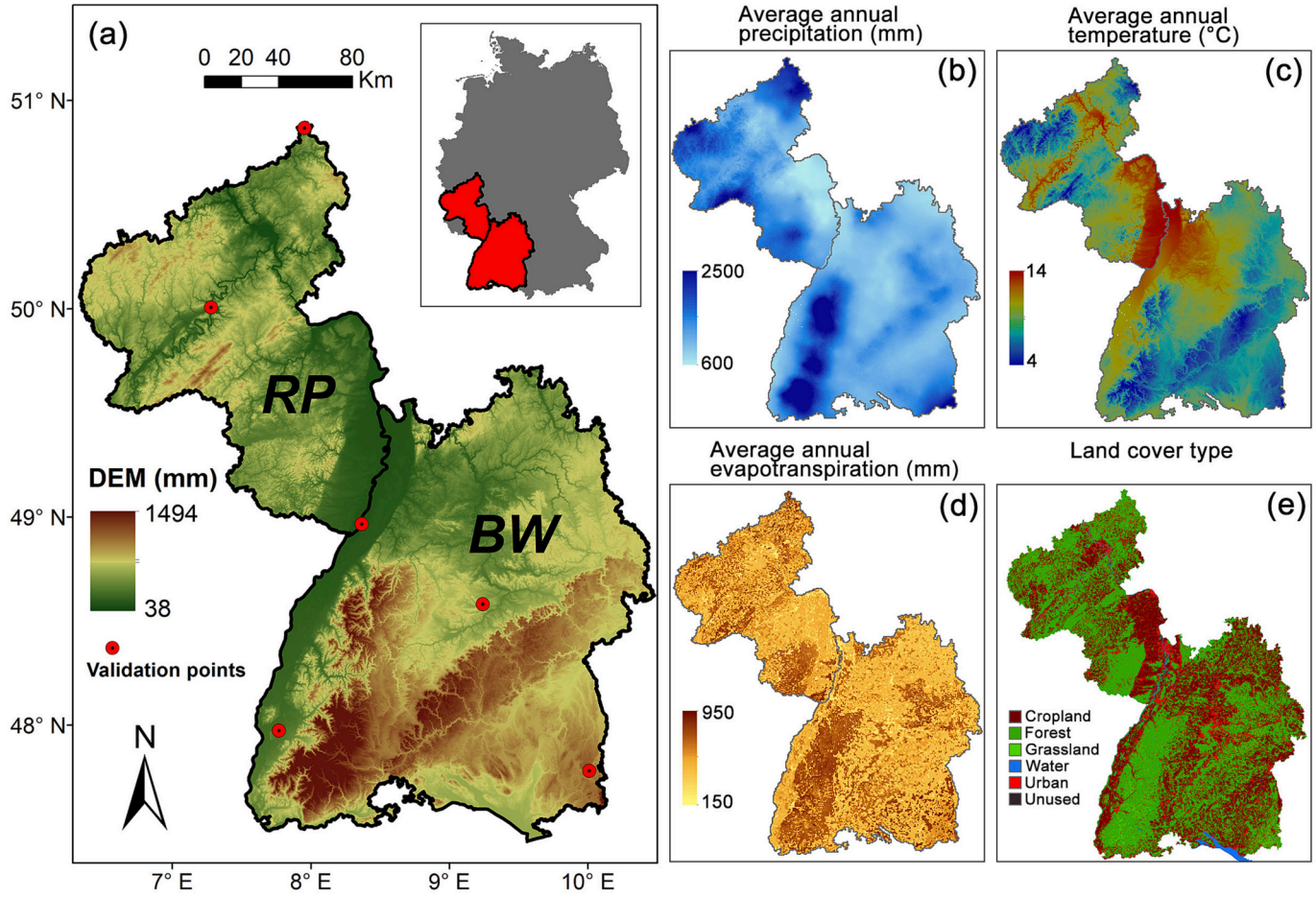

Fig. 1. (a) DEM and the selected grid points for model evaluation, (b) average annual precipitation, (c) air temperature, (d) TRAIN-simulated evapotranspiration (ET), and (e) land use type over the study area. Reference period is 1961–2016.

warm summers and mild winters with no dry seasons. The mean annual (1961–2016) total precipitation varied from below 600 mm on the leeward sites and depressions in the RP to approximately 2000 mm or more on the windward mountain slopes of the Black Forest in BW (Dong and Menzel, 2016; Liu and Menzel, 2016). The mean annual temperature ranges from approximately 4 °C on the highest peaks to 12 °C in the plains. The mean annual ET (calculated using the TRAIN model, as described later) ranged from 150 mm (residential areas and sealed surfaces) to 950 mm (open water surfaces), but typical values for natural vegetation ranged between 350 and 800 mm. In addition, six points (each point corresponding to a 1 × 1 km grid point in the TRAIN model) were selected to perform point-scale evaluation of the TRAIN model. They are distributed over typical landscapes, such as river valleys, plains, woodlands, and mountains (Fig. 1).

2.2. Data

The data used in this study comprised two main parts. The first category was used to drive the TRAIN model (see Section 3), which includes meteorological data (air temperature, precipitation, solar radiation, relative humidity, sunshine duration, and wind speed) and physiological information (Digital Elevation Model, land cover, and soil properties). The meteorological data used in this study, spanning from 1961 to 2016, were obtained from gridded data provided by the Climate Data Center of the German Weather Service (DWD, ftp://opendata.dwd.de/climate_environment/CDC/). All daily meteorological data were then interpolated to 1 km × 1 km resolution grids covering the RP and BW states. For the geographic information, gridded elevation data (1 km × 1 km resolution) were obtained from the Federal Agency for Cartography and Geodesy (http://www.geodatenzentrum.de). Land cover information (30 m resolution) was retrieved from the EU-wide project Corine 2006 data set (https://land.copernicus.eu/pan-european/corine-land-covera). Soil property data (such as the field capacity and depth of the root zone; scale of 1:50000 m) were derived from the Federal State Office for Geology, Raw Materials and Mining of BW (https://www.lgrb-bw.de/aufgaben_lgrb/geola), as well as from the Federal State Office for Geology and Mining RP (https://www.lgb-rlp.de/startseite.html). Land cover and soil property data were then interpolated based on the majority class within each 1 km × 1 km grid cell (Tijdeman and Menzel, 2021).

The second data category was used to evaluate the performance of the TRAIN model. The TRAIN model focuses on the simulation of fluxes at the soil-vegetation-atmosphere interface, such as ET and RZSM. Therefore, two ET and three SM product datasets were selected for comparisons with TRAIN-based simulations of ET and RZSM. Detailed information regarding these evaluation datasets is presented in Table 1.

Table 1
Information on the selected evapotranspiration (ET) and root zone soil moisture (RZSM) datasets used in this study.

Variables	Products	Temporal resolution	Spatial resolution	Period	Website
ET	ERA5-Land	Hourly	0.1° × 0.1°	1980–2016	https://cds.climate.copernicus.eu/
	GLEAM	Daily	0.25° × 0.25°	1980–2016	https://www.gleam.eu/
RZSM	SMAP-L4	3-hourly	9 × 9 km	2015–2016	https://nsidc.org/data/smap/data
	ERA5-land	Hourly	0.1° × 0.1°	1980–2016	https://cds.climate.copernicus.eu/
	GLEAM	Daily	0.25° × 0.25°	1980–2016	https://www.gleam.eu/

The ERA5-Land reanalysis dataset was developed by the European Centre for Medium-Range Weather Forecasts (ECWMF) based on the ERA5 land surface component, with a series of improvements and recalculations. ERA5-Land has a spatial and temporal resolution of 1 h and 0.1°, respectively, and is used worldwide (Liu et al., 2020a, 2020b; Muñoz-Sabater et al., 2021). The GLEAM ET dataset was generated using a set of algorithms based on the Modified Priestley–Taylor equations. Since its development in 2011, the model has been revised regularly (Martens et al., 2017) and has been widely applied (Jiang et al., 2021).

The SMAP-L4, ERA5-Land, and GLEAM soil moisture datasets were based on remote sensing, reanalysis, and fusion technologies, respectively. The SMAP dataset provides direct sensing of the soil moisture in the top 5 cm of the soil column. However, RZSM in the top 1 m of the soil column cannot be directly measured using SMAP. To fill this gap, SMAP developed 3-hourly estimates of soil moisture at a resolution of 9 km, i.e., the SMAP-L4 SM product, by merging SMAP observations with estimates from a land surface model in a data assimilation system. The volumetric soil moisture content in the ERA5-Land reanalysis dataset was simulated for four layers: 0–7, 7–28, 28–100, and 100–289 cm. According to the prevailing vegetation and average rooting depths, we assumed that the soil moisture could meet the demands of vegetation up to a soil depth of 100 cm. Thus, we chose the soil moisture information at a depth of 100 cm. The weighted average of the first three soil moisture layers was calculated. Finally, the RZSM in the GLEAM dataset was calculated using a multi-layer water-balance algorithm considering net precipitation (precipitation minus interception loss) and snowmelt as inputs and ET and drainage as outputs (Miralles et al., 2011). The depth of the root zone is a function of the land cover type and comprised three model layers for the fraction of tall vegetation (0–10, 10–100, and 100–250 cm), two model layers for the fraction of low vegetation (0–10 and 10–100 cm), and one model layer for the fraction of bare soil (0–10 cm).

To maintain consistency in the spatial and temporal resolution for the evaluation of the TRAIN model, ERA5-Land and GLEAM data from 1980 to 2016 were unified to a daily scale and interpolated to a 1 km × 1 km resolution grid using the inverse distance weighting (IDW) method. As the SMAP-L4 dataset starts on 31 March 2015, we used the datasets (listed in Table 1) from 2015.03.31 to 2016.12.31 to evaluate the daily RZSM simulated by the TRAIN model.

3. Model and methods

3.1. TRAIN model

The TRAIN (TRAnspiration and INterception indicating the major processes considered during the initial phase of model development) model, developed by Menzel (1996, 1997), is a hydrological model based on soil–vegetation–atmospheric transfer schemes (SVATS) and has been applied and validated in Switzerland (Menzel et al., 1999), Jordan (Menzel et al., 2009; Törnros and Menzel, 2014), and southwestern Germany (Stork and Menzel, 2016; Tijdeman and Menzel, 2021). The model includes information from comprehensive field studies on the water and energy balance for different surface types, such as snow, ET, interception, soil moisture, and runoff. It can simulate the spatial patterns of individual water budget components at different spatial and temporal scales. Typical applications are at point and regional scales, with temporal resolutions of one hour or one day. The model required precipitation, global or net radiation, soil heat flux (if available), air temperature, relative humidity, and wind speed as inputs. Information regarding the soil depth, water-holding capacity of the soil, leaf area index (LAI), and vegetation height is also essential for the model. If LAI and/or vegetation height information is not available, the model makes appropriate assumptions, such as the typical development of LAI or vegetation height for the respective vegetation. The outputs of

the TRAIN model included interception evaporation, transpiration, total evapotranspiration, root zone soil moisture, percolation, runoff, and snow cover.

As shown in Fig. 2, the TRAIN model typically considers four processes: snow store change, interception and ET, soil moisture change, and runoff generation. The core of the model is the simulation of ET and soil moisture. In the TRAIN model, transpiration is generally calculated based on the Penman–Monteith equation (PM), using a model to simulate the canopy resistance, r_c. The PM equation can be described as follows:

$$\lambda E = \frac{\triangle(R_n - G) + \rho c_p D_{ref}/r_a}{\triangle + \gamma(1 + r_c/r_a)} \quad (1)$$

where E is the vapour flux ($kg{\cdot}m^{-2}\ s^{-1}$), λ is latent heat of vaporisation ($J{\cdot}kg^{-1}$), R_n is net radiation ($J{\cdot}m^{-2}\ s^{-1}$), G is soil heat flux ($J{\cdot}m^{-2}\ s^{-1}$), Δ is the slope of the saturation vapour pressure ($hPa{\cdot}K^{-1}$), γ is a psychometric constant ($(hPa{\cdot}K^{-1})$), ρ is the density of dry air ($kg{\cdot}m^{-3}$), c_p is the special heat of dry air ($J{\cdot}kg^{-1}\ K^{-1}$), D_{ref} is the specific humidity deficit at a reference height (hPa), r_a is the aerodynamic resistance ($s{\cdot}m^{-1}$), and r_c is the canopy resistance ($s{\cdot}m^{-1}$). Specifically, r_c is modified by vegetation growth, soil moisture status, and weather conditions (Menzel, 1996):

$$r_c(T, LAI, \delta\theta) = a_0 + a_1 r_c(T) + a_2 r_c(LAI) + a_3 r_c(\delta\theta) \quad (2)$$

$$r_c(T) = (T + b_1)^4 \quad (3)$$

$$r_c(LAI) = exp(b_2 LAI) \quad (4)$$

$$r_c(\delta\theta) = (\delta\theta + b_3) \quad (5)$$

where T is the air temperature (°C); LAI is the Leaf area index; $\delta\theta$ is the soil moisture deficit (mm); and a_0, a_1, a_2, a_3, b_1, b_2, and b_3 are regression coefficients. According to Menzel (1997), the maximum amount of water that can be stored in the canopy depends on the seasonal development of the LAI, and interception evaporation is modelled to occur at different intensities as a function of the actual amount of water accumulated in the canopy and present weather conditions.

In addition, the calculation of the soil water status and percolation in the TRAIN model follows the conceptual approach of the Hydrologiska Byråns Vattenbalansavdelning (HBV) model (Bergström, 1995), in which the soil column is not subdivided into different layers but is understood as one uniform soil column. Soil moisture was calculated by balancing precipitation and ET, using field capacity and permanent wilting points as parameters. The calculation process is as follows:

$$\frac{Q}{P} = \left(\frac{SM}{F_C}\right)^{\beta} \quad (6)$$

where Q/P is often called the runoff coefficient, SM is the soil moisture (mm), F_C is the maximum soil moisture storage (mm), and β is a shape parameter associated to soil characteristic. A weighing procedure was applied to obtain a single value from all soil moisture measurements within one profile. The contribution of each soil measurement depth was weighted and summed with respect to the depth within the total soil column. Therefore, the soil moisture in the TRAIN model was considered to be RZSM. For more information on the TRAIN model and its applications, please refer to Stork and Menzel (2016) and Tijdeman and Menzel (2021).

3.2. Identification of flash drought

As recommended by Otkin et al. (2018), a definition of "flash drought" should inherently account for both its rapid intensification (i.

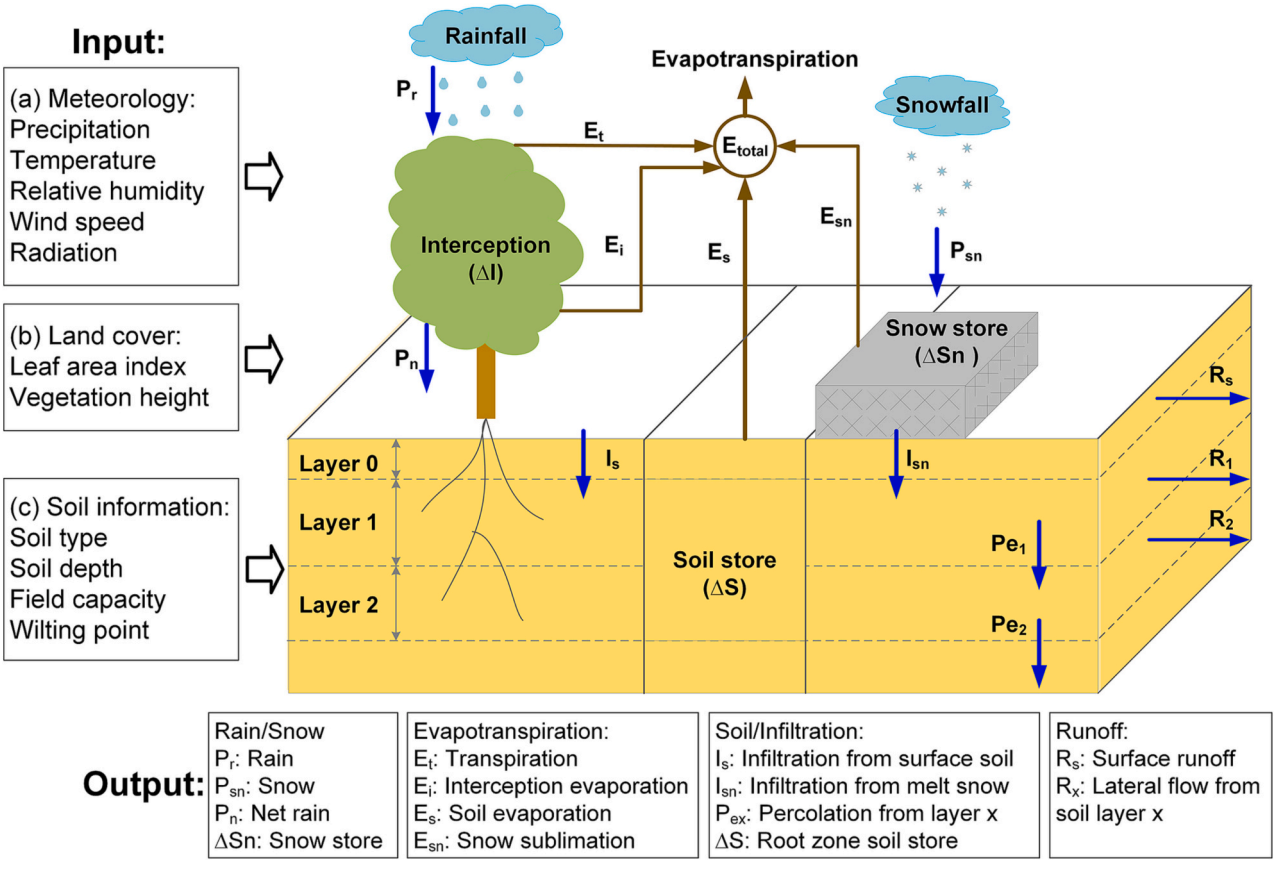

Fig. 2. Flow chart of the TRAIN model.

e., the flash) and the actual condition of moisture limitation (i.e., the drought). Fig. 3 illustrates the flash drought event identification method used in this study. The RZSM was selected for the identification of flash droughts, and a flash drought event should meet the following conditions:

(1) A flash drought onset when the RZSM dropped from greater than or equal to the 40th percentile to less than or equal to the 20th percentile, with a decline rate greater than or equal to the 10th percentile for each pentad.

(2) A flash drought terminates when the RZSM is greater than or equal to the 20th quantile for at least two pentads.

(3) The duration of a flash drought should range from 6 to 18 pentads. If the duration was <6 pentads, we considered it a short-term dry event; if the duration was >18 pentads, we considered it a conventional slowly evolving drought event.

In addition, the aim of this study was to explore changes in flash droughts under the impact of heat waves. According to previous studies (Skrzyńska and Twardosz, 2022; Hartmann et al., 2023; Rouges et al., 2023), the vast majority of heat waves in southwestern Germany are restricted to the summer season (from June to August). Therefore, we mainly focused on flash droughts that occurred during the summer season and all flash droughts mentioned below refer to summer flash droughts. Furthermore, according to the previous researches (Zou et al., 2018; Wang et al., 2022), the Gamma distribution function was selected to fit the probability distributions for the flash drought duration and onset speed. The Kolmogorov-Smirnov (K-S) (Massey, 1951) test method was adopted to determine the effectiveness of the fitting. The value p calculated by the K-S test could reflect the confidence level of the fitting results. Usually, the fitting result could pass the significant level test when the p value is >0.05, and the closer the p value is to 1, the higher the confidence level is.

3.3. Identification of heat wave events

Air temperature is an important factor in the definition of heat waves because of its near-ubiquitous measurement and direct impact (Liu et al., 2020a). Climate communities consider heat waves to be multi-characteristic events, including intensity, duration, and frequency (Perkins, 2015). Consequently, many definitions of heat waves based on air temperature have been proposed that incorporate different intensity or duration thresholds. For example, Vautard et al. (2013) analysed both the amplitude and persistence of European heat waves based on the 90th percentile of the daily mean air temperature. Schoetter et al. (2015) defined a heat wave as a period in which the maximum temperature was above the 98th percentile for at least three days. In this study, we selected the heat waves identification methods recommended by the World Meteorological Organization (WMO) to define heat waves days as periods of at least five consecutive days in the summer season (from June to August) when the daily maximum temperature exceeded the climatological average of at least 5 K for the 1961–1990 reference period. According to the statistical results, ranges of the mean and max durations of heat wave events for all the grids in BW (RP) state are 5.89–8.82 days and 9.00–19.00 days (5.80–8.42 days and 14.00–17.00 days), respectively, which are approximately equal to 1–2 pentads and 2–3 pentads, respectively. At the same time, there may be some lag effect in the impact of heat waves on flash droughts. Therefore, in this study, if a heat wave event occurred at the same time or within three pentads prior to a flash drought event, we considered that the heat wave event met this flash drought event. Due to the rapid development of a flash drought, if a heat wave event occurs after the onset of a flash drought, it primarily affects the termination process of the flash drought rather than the onset process, and we do not focus on such encounters.

3.4. Trend analysis method

The Mann-Kendall (MK) trend test method (Mann, 1945; Kendall, 1975), recommended by the World Meteorological Organization (WMO), is a widely used nonparametric test method to determine trends of hydrological or meteorological series (e.g., precipitation, temperature, and streamflow). For a time series of n observations $X = x_1, x_2, \ldots, x_n$, the statistic value Z is estimated as follows:

$$Z = \begin{cases} (S-1)\Big/\sqrt{var(S)}, & S > 0 \\ 0, & S = 0 \\ (S+1)\Big/\sqrt{var(S)}, & S < 0 \end{cases} \quad (7)$$

where,

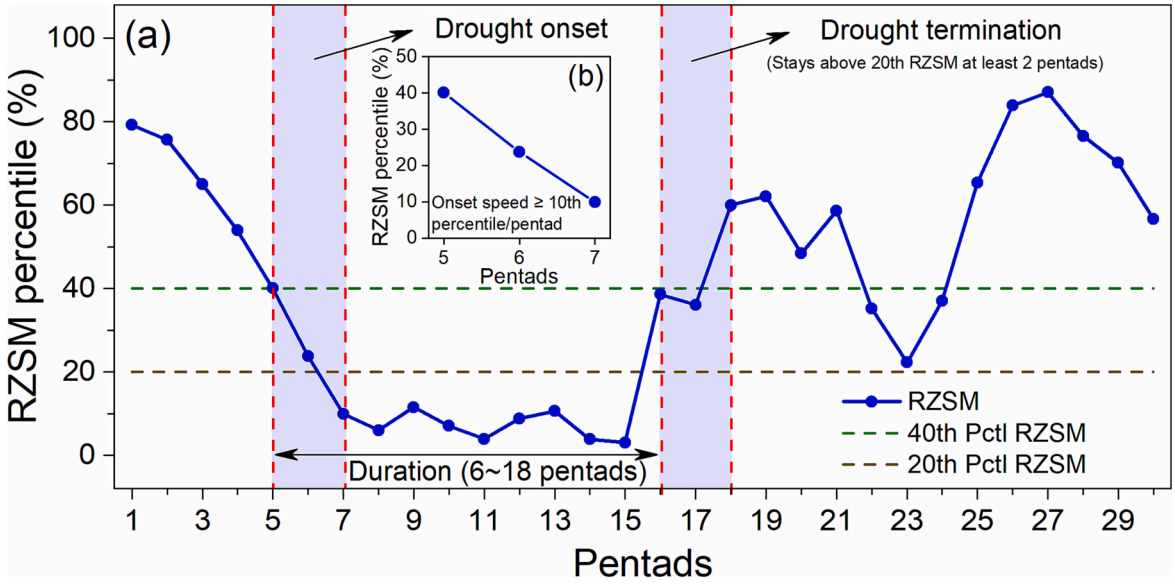

Fig. 3. Schematic of the identification process of flash drought indicated by the root zone soil moisture (RZSM) percentile. (a) Whole phase of a flash drought event; the RZSM (the blue solid line) decreases from above the 40th percentile (the green-dashed line) to below the 20th percentile (the brown-dashed line). The first and second purple shaded areas represent the onset and termination phase of a flash drought, respectively. (b) Schematic representation of the onset phase of a flash drought event with an average decline rate of no less than the 10th percentile for each pentad.

$$S = \sum_{i=1}^{n-1} \sum_{j=i+1}^{n} sgn(x_j - x_i) \tag{8}$$

$$sgn(\theta) = \begin{cases} +1, & \theta > 0 \\ 0, & \theta = 0 \\ -1, & \theta < 0 \end{cases} \tag{9}$$

The variance of S is computed as follows:

$$var(S) = n(n-1)(2n+5)/18 \tag{10}$$

where, x_i and x_j are the corresponding sample values for years i and j, respectively, and a positive value of Z (i.e., $Z > 0$) denotes an upward trend, and the opposite ($Z < 0$) corresponds to a downward trend. In this study, we selected 0.05 (i.e., $|Z| > 1.96$) as the statistical significance threshold to determine the upward and downward trends.

4. Results

4.1. Evaluation of TRAIN simulated ET and RZSM

First, we conducted spatial analysis to evaluate the performance of the TRAIN model simulation. Figs. 4(a) and (b) show that the ET simulated by the TRAIN model was most highly correlated with the ERA5-Land ET data, followed by the GLEAM ET data, with average basin correlation coefficients of 0.828 and 0.803, respectively. Figs. 4 (c)-(e) show that the RZSM simulations of the TRAIN model had the highest correlation with the ERA5-Land data, followed by the SMAP-L4 and GLEAM data. The regional average correlation coefficients were 0.765, 0.746, and 0.762, respectively. For the GLEAM data, the region with the lowest correlation was concentrated in the central part of the BW state. For the SMAP-L4 data, the lower correlation area was located in the southern part of the state of BW. The topography of the two areas is mountainous, and the land cover type is mainly forest (i.e., the Black Forest). Special topography and vegetation cover may lead to more uncertainties and errors in the model simulations and satellite observations associated with the RZSM, resulting in low correlation coefficients between the TRAIN model simulation results and the other three datasets. Overall, the correlation values between the TRAIN model simulated variables (ET and RZSM) and the other three datasets were high for most parts of the study area.

We then selected six sample points (Fig. 1(a)) to further evaluate the performance of the ET and RZSM simulated by the TRAIN model on a

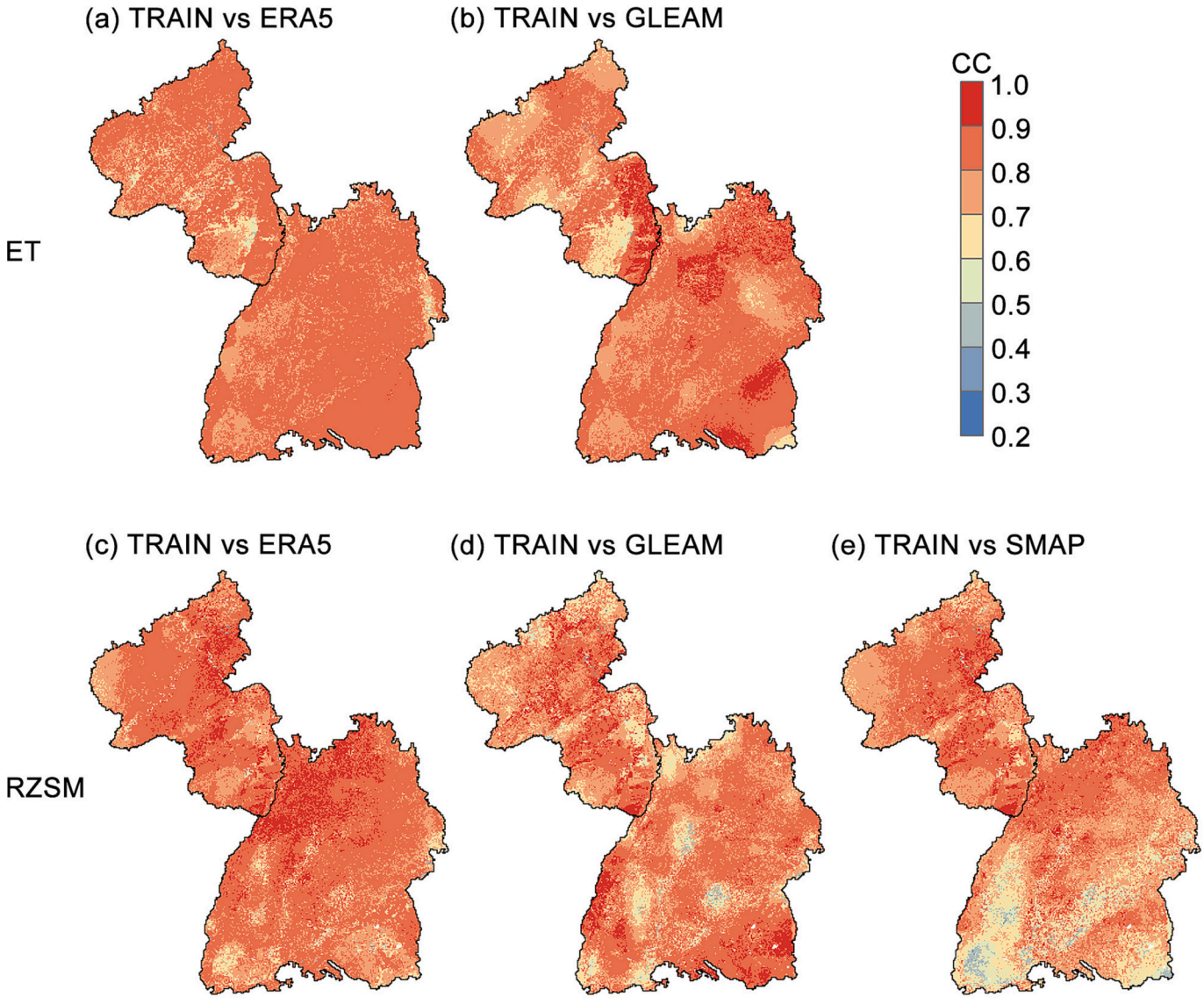

Fig. 4. Spatial evaluation of the ET ((a)–(b)) and RZSM ((c)–(e)) simulated by TRAIN from 1980 to 2016 for the ERA5 and GLEAM dataset, as well as from 2015 to 2016 for the SMAP dataset.

point scale (Fig. 5). TRAIN simulated ET (left side of Fig. 5) exhibited the same seasonality as the ET produced by the ERA5 and GLEAM datasets, with correlation coefficients of 0.78–0.88 with the ERA5 dataset and 0.71–0.87 with the GLEAM dataset. The time series on the right side of Fig. 5 show good correspondence between the TRAIN simulated RZSM and the RZSM produced by the ERA5, GLEAM, and SMAP datasets. The correlation coefficients of the TRAIN simulated RZSM with the three datasets ranged from 0.78 to 0.90 (ERA5), 0.78–0.92 (GLEAM), and 0.72–0.93 (SMAP). These evaluation results indicate that the TRAIN model can reasonably simulate the ET and RZSM across the study area. Thus, the simulated data can be used for the further identification of flash droughts.

4.2. Temporal and spatial changes in flash drought and heat waves

Figs. 6(a), (b), (g), and (h) show the number of flash drought and heat wave events per year averaged over the BW and RP states from 1961 to 2016. Anomalies in the annual mean temperature, precipitation, ET, and RZSM were also calculated (Figs. 6(c)–(f) and (i)–(l)). In the years around 1990 (1988–1992), both the BW and RP states experienced consecutive anomalously high temperatures and ET and persistently anomalously low precipitation and RZSM, leading to a peak in the number of flash droughts in 1990.

The temporal trends in these series were then analysed using the Mann-Kendall trend test method. The results showed that the number of heat waves, flash drought events, annual temperature, and ET in the BW and RP regions showed significant increasing trends ($p < 0.05$). Precipitation and RZSM in these two regions showed a non-significant decreasing trend ($p > 0.05$).

Furthermore, Figs. 7(a) and (e) show the spatial distributions of the frequencies of heat waves and flash droughts in the BW and RP states during the entire study period (1961–2016). Figs. 7(b), (c), (f), and (g) show comparisons of the frequency of heat waves and flash droughts between the base period of 1961–1990 (base period usually recommended by the World Meteorological Organization for climate change studies) and the comparison period of 1991–2016. The frequency of heat waves and flash droughts increased in most regions during the comparison period compared with the base period. Figs. 7(d) and (h) show the percentage change in frequency for heat waves and flash droughts between the two periods, respectively. In the RP region, the increase in the heat waves frequency was within 0–200 % in most areas, whereas in the BW region, the increase in heat waves frequency was >300 % in most areas. The increase in the flash drought frequency was >40 % in most areas of the RP and BW regions.

Fig. 8 shows the decadal variations in the number of heat waves, flash droughts, and the coincidence of these two events. From a median value perspective, the number of heat waves in the BW (Fig. 8(a)) continuously increased while the number of flash drought events (Fig. 8

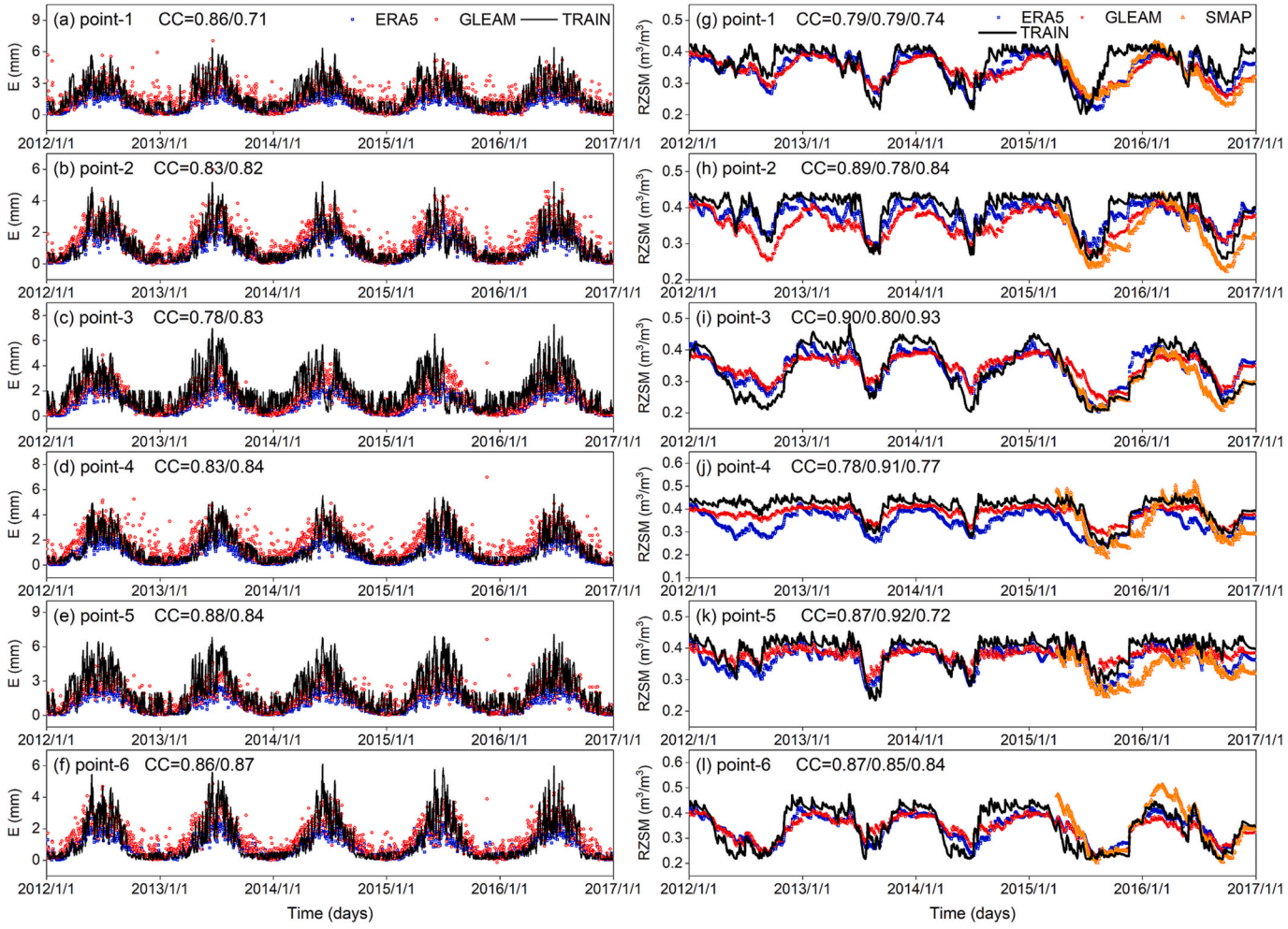

Fig. 5. Point evaluation of the ET and RZSM simulated by TRAIN. The spatial distributions of the six points (point-1 to point-6) can be found in Fig. 1. CC values on the left side of the figure ((a)–(f)) are correlation coefficients between the evapotranspiration (ET) simulated by the TRAIN model and ET produced by ERA5 and GLEAM from 2012 to 2016, respectively. CC values on the right side of the figures ((g)–(l)) are correlation coefficients between the root zone soil moisture (RZSM) simulated by the TRAIN model and RZSM produced by ERA5 and GLEAM from 2012 to 2016 and SMAP from 2015 to 2016, respectively.

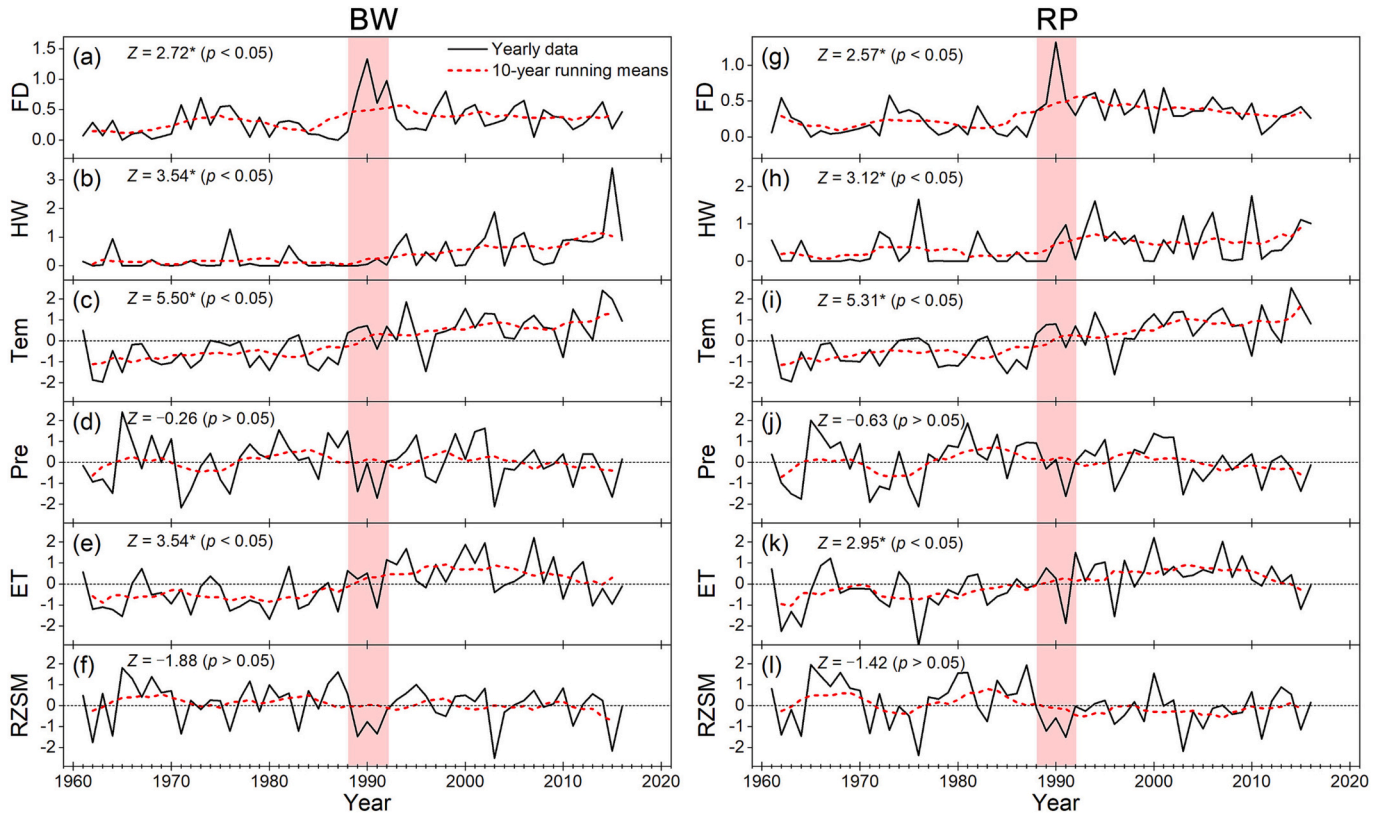

Fig. 6. Regional average annual and decadal variations in flash and heat wave events and their component variables across the study area. (a) and (g) The number of flash drought (FD) events per year; (b) and (h) the number of heat waves (HW) events per year; (c) and (i) temperature (Tem) anomaly, (d) and (j) precipitation (Pre) anomaly, (e) and (k) evapotranspiration (ET) anomaly, and (f) and (l) root zone soil moisture (RZSM) anomaly. Except for the number of flash drought and heat wave events ((a), (b), (g), and (h)), the component variables ((c)–(f) and (i)–(l)) are standardized before being averaged to facilitate the comparison. The *Z* values are the Mann-Kendall test results; Z values reaching the 0.05 significance level ($p < 0.05$) are marked with an asterisk. The pink shaded area covers the year (i.e., 1990) when the peak of the flash drought numbers appeared and its adjacent years.

(b)) increased in the first four decades and then remained constant. The coincidence number of these two events (Fig. 8(c)) also increased continuously. As for the RP state, the number of heat waves, flash droughts, and the coincidence of these two events (Fig. 8(d)–(f)) almost increased and then decreased, showing a different change characteristic compared to the BW state.

4.3. Assessment of the impact of heat waves on flash drought processes

Fig. 9 shows a comparison between the two types of flash droughts. Figs. 9(a)–(d) show the changes in the pentad-scale percentile of the RZSM, precipitation, ET, and maximum temperature in an independent flash drought event that did not coincide with a heat wave event. We defined this type of flash drought as FD-I. The changes in Figs. 9(e)–(h) occurred during a compound event in which a flash drought event met with a heat wave event. We defined this type of flash drought as FD-II. Both flash drought events (FD-I and FD-II) experienced similar precipitation deficits (Figs. 9(b) and (f)). The difference is that FD-I did not encounter a heat wave event and had a slow regional translation in maximum temperatures from anomalously low to high (Fig. 9(d)), whereas FD-II encountered a heat wave event with the regional maximum temperatures having a rapid translation from anomalously low to high and then to low (Fig. 9(h)). Different temperature translation led to different ET change processes. The ET of FD-I (Fig. 9(c)) experienced a slow translation from anomalously low to high, and then gradually reached extreme values. However, the ET of FD-II (Fig. 9(g)) showed a rapid shift from anomalously low to high values and then returned to a low value. Changes in the RZSM for the two types of flash droughts also differed. The RZSM of the FD-I (Fig. 9(a)) gradually translated from a surplus to a deficit. However, the RZSM of FD-II (Fig. 9 (e)) showed a rapid shift from surplus to serious deficit and continued to remain under serious deficit conditions for an extended period, even after the heat wave event had finished.

The statistical and probabilistic fitting results for the flash drought duration and onset speed for FD-I and FD-II events in BW and RP states are showed in Fig. 10. All the Gamma probability fitting distribution results passed the KS significance test, i.e. $p > 0.05$ (Figs. 10(a)-(h)). The results showed statistically significant differences in the flash duration and onset speed rate of FD-I and FD-II. Specifically, in BW state (Fig. 10 (i)), the mean flash drought durations of FD-I and FD-II were 10.42 and 8.95 pentads, respectively, and the corresponding values in RP state (Fig. 10(k)) were 10.67 and 9.53 pentads, respectively. The mean flash drought onset speed for the BW state (Fig. 10(j)) was the 19.69th percentile/pentad for FD-I and 21.77th percentile/pentad for FD-II, respectively; the corresponding values for the RP state (Fig. 10(l)) were the 17.16th percentile/pentad for FD-I and 19.91th percentile/pentad for FD-II, respectively. These results indicate that heat wave events may shorten the duration of flash droughts and accelerate the onset speed of flash droughts.

Here, we analysed the changes in the hydro-meteorological variables before and after the onset of two types of flash droughts (FD-I and FD-II). Figs. 11(a) and (e) show that in the BW and RP states, the median values of the precipitation box for both types of flash droughts were above or near the 50th percentile before the onset of the flash droughts and then fell below the 40th percentile after the onset of the flash droughts. Figs. 11(b) and (f) show that the median values of the maximum temperature box for both types of flash drought in the BW and RP states were near or below the 50th percentile before the onset of the flash

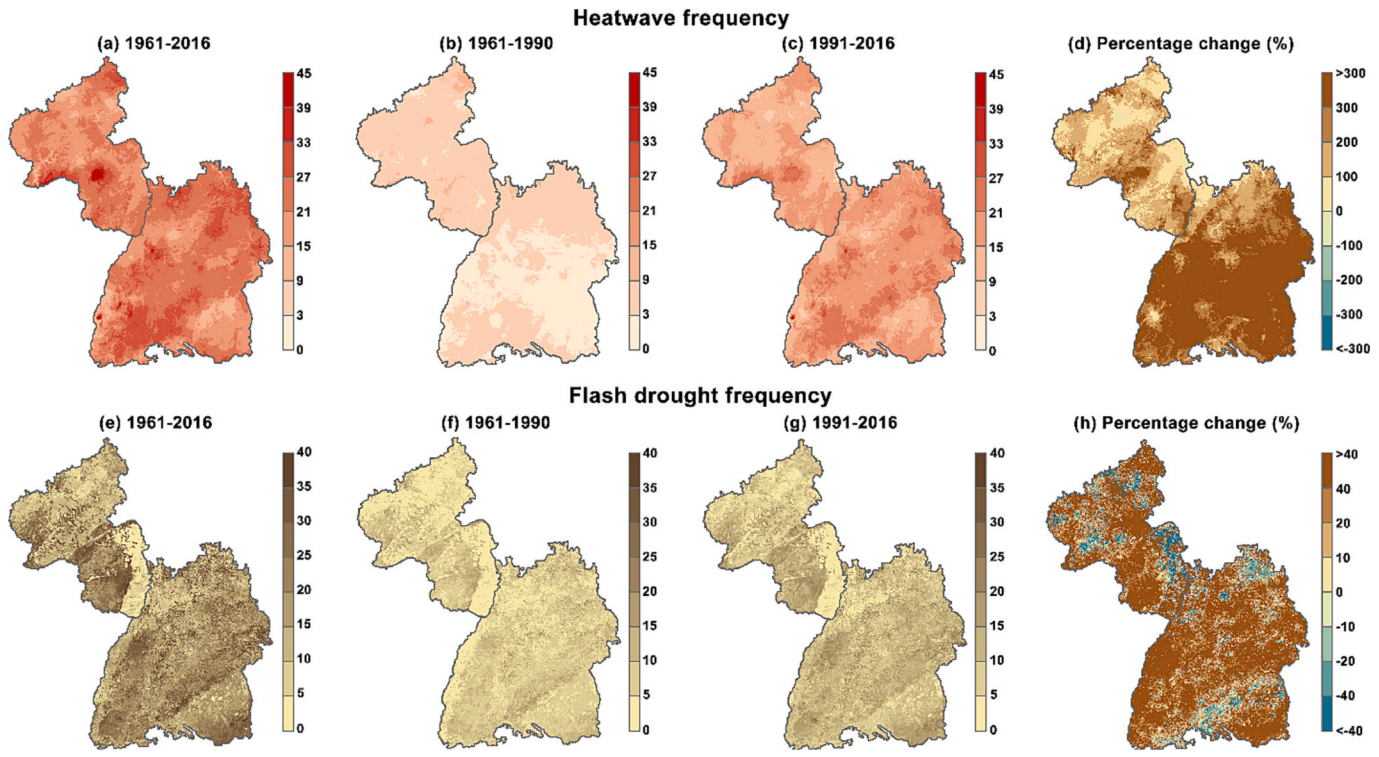

Fig. 7. Spatial frequency of heat waves and summer flash drought events from 1961 to 2016 ((a) and (e)), 1961–1990 ((b) and (f)), and 1991–2016 ((c) and (g)), and their percentage changes from 1991 to 2016 relative to 1961–1990, i.e., ((post-1990–pre-1990)/pre-1990) × 100.

droughts. After the onset of flash droughts (from lag+1 to lag+3), all median values of the box for FD-II were above the 70th percentile, whereas those for the FD-I drought were around or below the 60th percentile. Figs. 11(c) and (g) show that the median value of the ET Box for both types of flash droughts tended to increase during the period from lag–3 to lag+1, and then decreased from lag+1 to lag+3. The difference was that for each pentad before and after the onset of flash droughts, the median values of the ET Box for FD-II were higher than those for FD-I. Figs. 11(d) and (h) show that the median values of the RZSM box for both types of flash droughts were above the 50th percentile before the onset of the flash drought. After the onset of the flash drought (from lag+1 to lag+3), all median values of the RZSM box for both types of flash drought decreased from the 50th percentile to the 20th percentile. However, for each pentad, after the onset of the flash droughts, the median values of the RZSM Box for FD-II were lower than those for FD-I. In particular, in the third pentad after the onset of flash drought (i.e., lag+3), almost all values of the RZSM box (upper marginal 95 % quartile line) for FD-II were below the 20th percentile, whereas only approximately 75 % (upper quartile line) of the RZSM box values for FD-I were below the 20th percentile.

These analyses show that the precipitation conditions of both types of flash droughts were similar before and after the onset of flash droughts. However, temperature- and energy-control conditions significantly differed between the two types of flash drought before and after the onset of flash droughts owing to the intervention of heat waves, resulting in higher water consumption through ET, a more severe decrease in RZSM, and a faster onset speed for the FD-II drought than that of the FD-I drought.

5. Discussion

In this study, the states of BW and RP in southwestern Germany were selected as the study area to assess the impact of heat waves on flash droughts. The results of the study showed a non-significant decreasing trend in RZSM in the two states, as well as a significant increasing trend in the frequency of flash drought and heat waves events. These results are consistent with the recent findings on the trend of SM and agricultural drought characteristics in the European continent (Albergel et al., 2013; Feng and Zhang, 2015; Piles et al., 2019). For example, Almendra-Martín et al. (2022) found a general decreasing trend of SM, regardless of climate type but more intense in Eastern and Central Europe, as well as a general increase in the duration and intensity of extreme droughts over the European continent. In this study, the increasing frequency of flash drought and heat waves events is inextricably linked to variations in atmospheric regimes. The large-scale climatic conditions in both states are quite similar, mostly determined by the Azores High and Icelandic Low and the seasonal changes in their position. A westerly wind belt with wandering cyclones is located between the two pressure systems. The seasonal oscillation of this system in the north–south direction causes a dominance of cyclonic weather, with frequent passage of frontal systems during winter and calming of the cyclonic activity in summer, in favour of high-pressure persistent large-scale weather situations. Recently, more long-lasting, quasi-stationary, and high-pressure systems have been observed during the summer months (Coumou et al., 2015; Ionita et al., 2017). This atmospheric blocking no longer allowed for humid and cool western atmospheric flows, and made it difficult for soil moisture in the study area to be consistently replenished by precipitation, which leads to an increase in the frequency of flash droughts.

Furthermore, we can examine the physical processes driving the moisture balance of the land surface to understand mechanisms that can lead to the differences of flash drought with and without heat wave. Like other aspects of drought, precipitation deficit often plays an important role. Moisture flux away from the surface—evapotranspiration (ET)—can also play an important role in flash drought, thus driving feedbacks between the land and atmosphere (Pendergrass et al., 2020; Qing et al., 2022). For the flash drought with and without meeting a heat wave event, their initial precipitation deficit states are relatively close to each other. However, the intervention of the heat wave events could lead to an increase in regional energy input and an immediate and rapid increase in the ET, accompanied by a rapid depletion of RZSM (Wang and

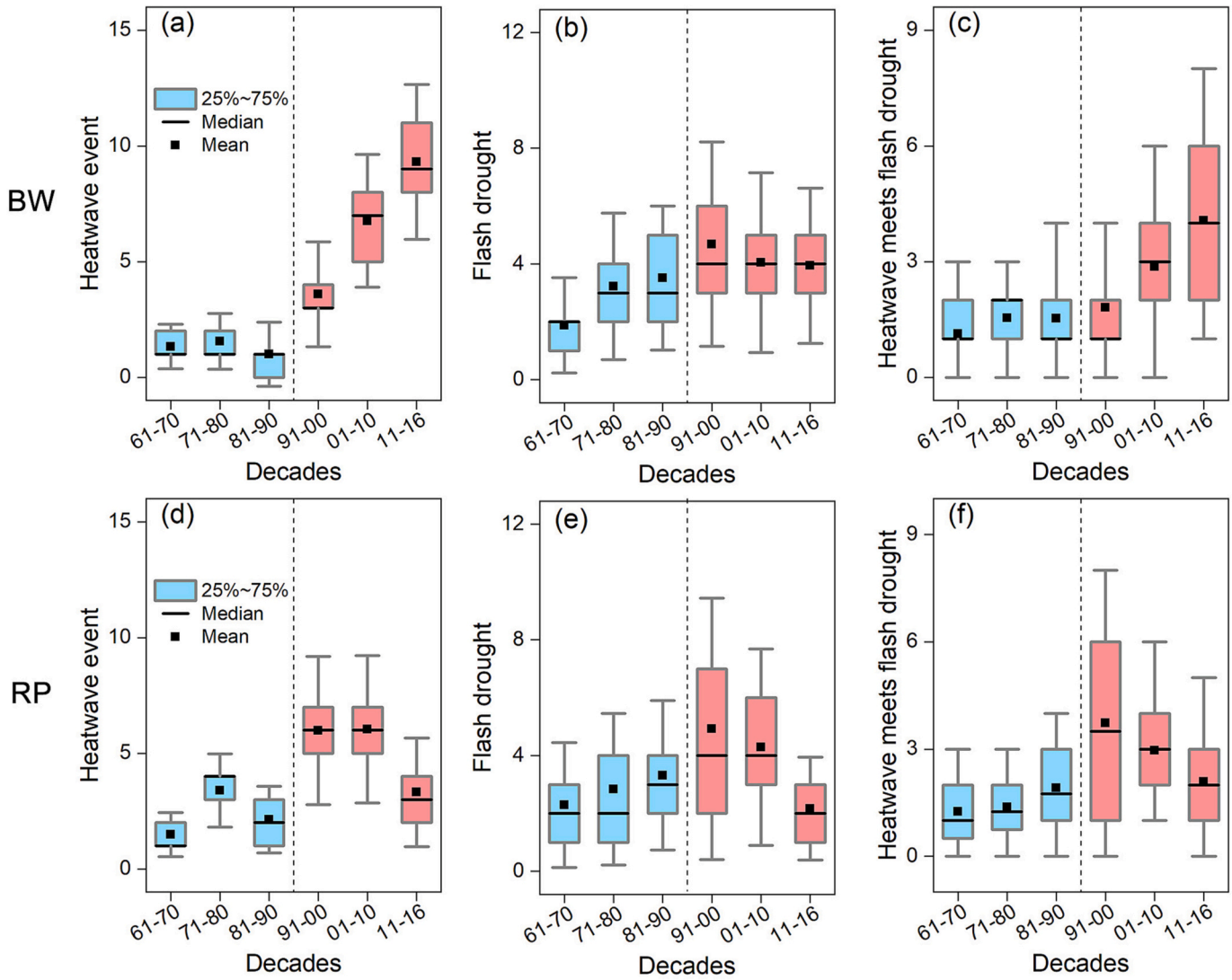

Fig. 8. Number of heat waves ((a) and (d)) and flash droughts ((b) and (e)), and the coincidence of these two events ((c) and (f)) during the past six decades for the Baden-Württemberg (BW) and Rhineland-Palatinate (RP) states.

Yuan, 2022). This causes an accelerated transition in the flash drought from the energy-limited stage (both temperature and ET increase) to the soil water-limited stage (temperature continues to increase while ET decreases), thus accelerating the onset speed of flash drought. Therefore, flash droughts under the influence of heat waves are generally shorter in duration but faster in occurrence.

Besides, we found differences even within a region of a relatively small spatial extent – BW and RP states together cover an area of approximately 55,000 km^2. We found some differences in the frequency of flash droughts and heat waves between the two states (Figs. 7 and 8), as well as different changes in the associated hydro-meteorological variables when flash droughts coincided with heat waves (Figs. 10 and 11). Topographic conditions may account for the above difference. On a smaller scale, the above mentioned atmospheric regimes is sometimes strongly modified by topographic conditions. The BW state is much more exposed to warm air inflows from southern directions, which move over the Rhone Valley (France), traverse the so-called Burgundian Gate to the Upper Rhine Valley (the lowlands in the far west of BW; see Fig. 1), and are often responsible for high air temperatures in BW state during summer. Therefore, differences in the influence of topographic conditions on the atmospheric regimes resulted in a higher frequency of heat wave events in BW state than in RP state.

In addition to topographic conditions, extremely spatially heterogeneous soil properties may contribute to the differences between the two states, including soil depth, soil type, and soil water-holding capacity. These findings have implications for land use. Previous studies (Hellebrand et al., 2009; Dong and Menzel, 2016; Liu and Menzel, 2016; Tijdeman and Menzel, 2021) have shown that the land cover types in BW, in descending order of percentage, are cropland (43 %), forest (38 %), grassland (10 %), urban (7 %), and water (2 %); in RP, it is forest (46 %), cropland (28 %), grassland (22 %), and urban (4 %). In both states, cropland prevails on deeper soils, which show a higher available water-holding capacity (AWC in millimetres; i.e., the amount of plant-available water in the root zone at field capacity), whereas shallow soils, disadvantageous for agriculture, are mostly covered by forests (Tijdeman et al., 2022). Compared with RP, BW had a higher proportion of croplands. It is mostly distributed in the lowlands, which are more strongly impacted by warm and hot air inflows. Moreover, emerging crops in deeper soils with high AWC likely consume more soil water during the transition from the energy-limited phase (increased ET and reduced RZSM) to the water-limited phase (simultaneous decline in ET and RZSM), resulting in a greater onset speed of flash drought and greater changes in ET and RZSM during the coincidence of flash droughts and heat waves. In summary, differences in topography, soil properties, and land cover appear to result in more pronounced changes in the frequency of heat waves and flash droughts in BW than in RP.

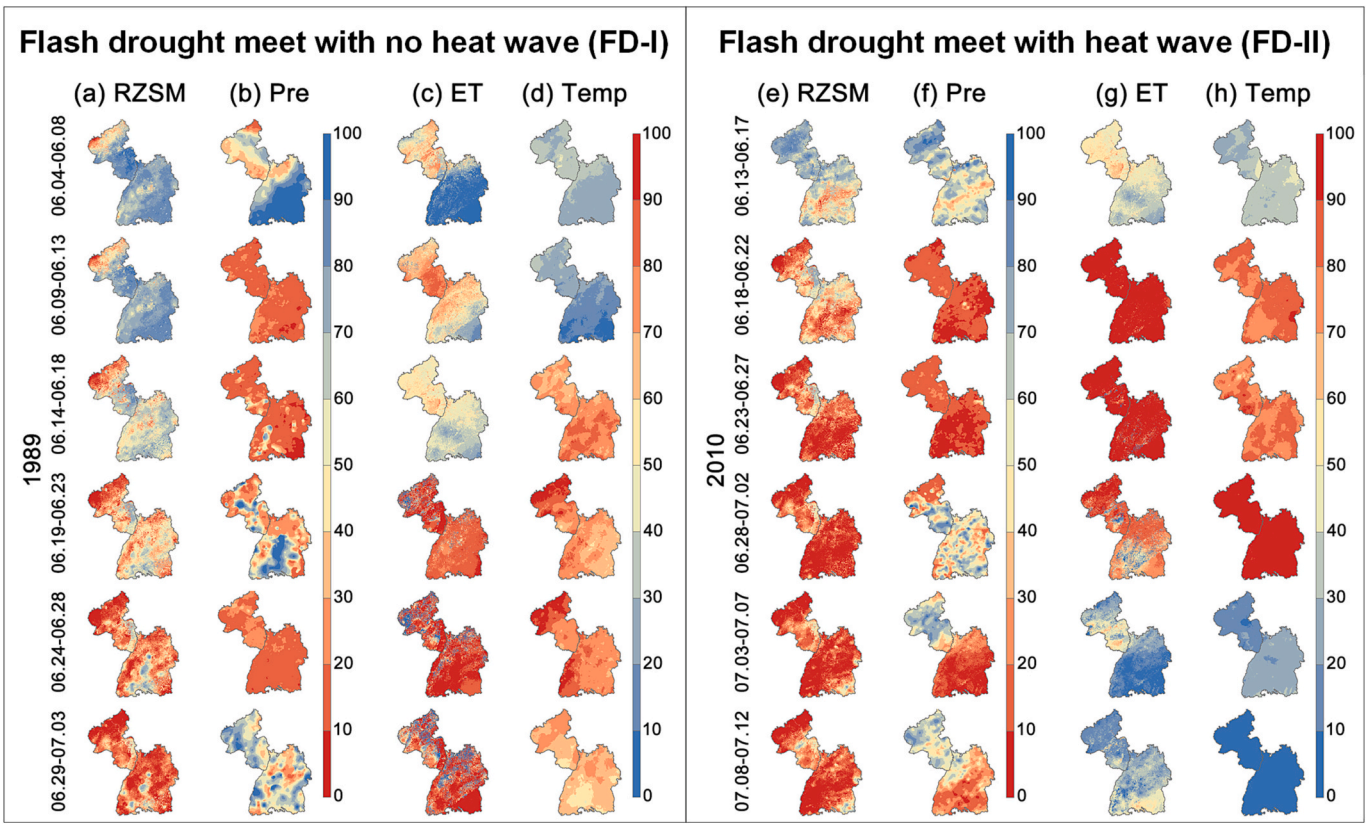

Fig. 9. Changes in the pentad-scale percentile of the root zone soil moisture (RZSM), precipitation (Pre), evapotranspiration (ET), and maximum temperature (Tmax) from 4 Jun–3 July 1989 ((a)–(d)) when a flash drought met with no heat wave event (we defined this type of drought as FD-I), and from 13 June–12 July 2010 ((e)–(g)) when a flash drought met with a heat wave event (we defined this type of drought as FD-II).

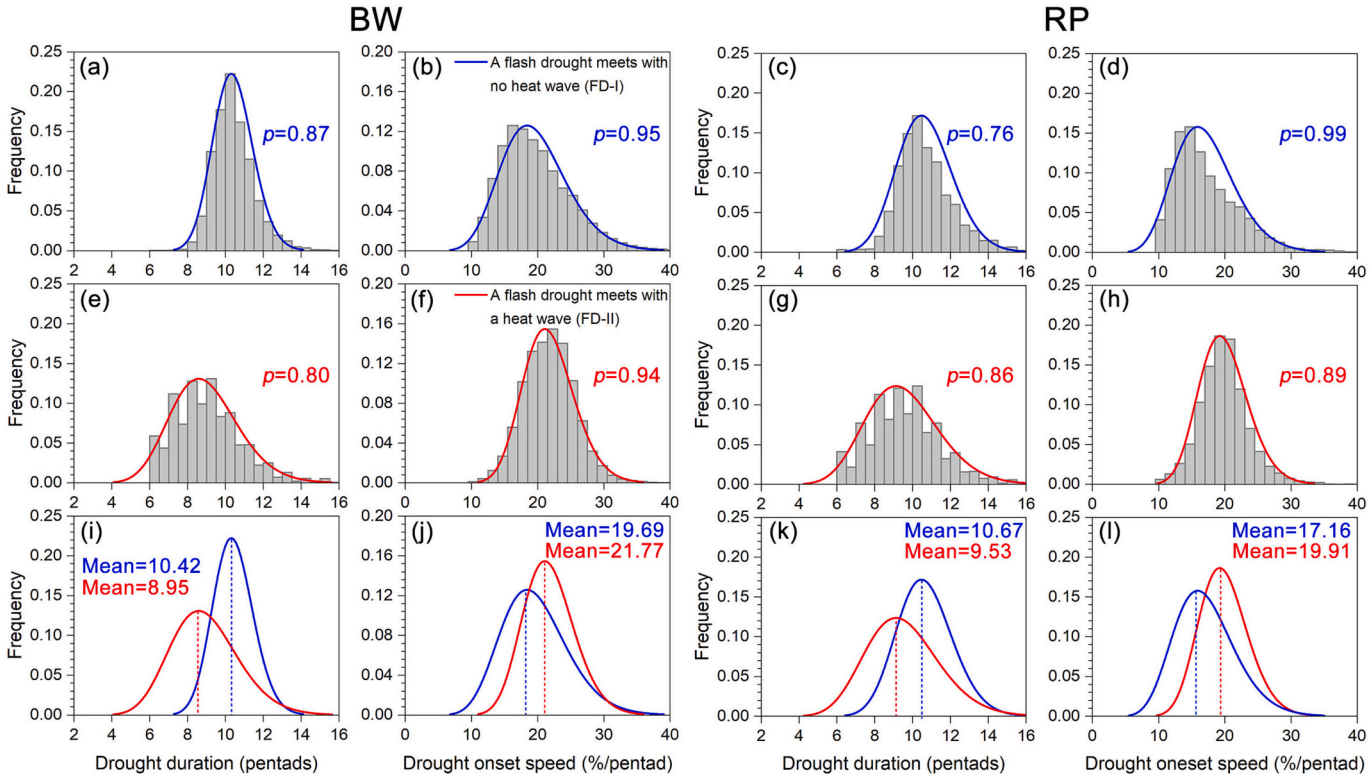

Fig. 10. Comparisons of the drought duration and onset speed between the two types of flash drought events, i.e., a flash drought meets (FD-I) with or without (FD-II) a heat wave event (the *p* values reflect the confidence level of the Kolmogorov–Smirnov test, and mean values are the average of all samples).

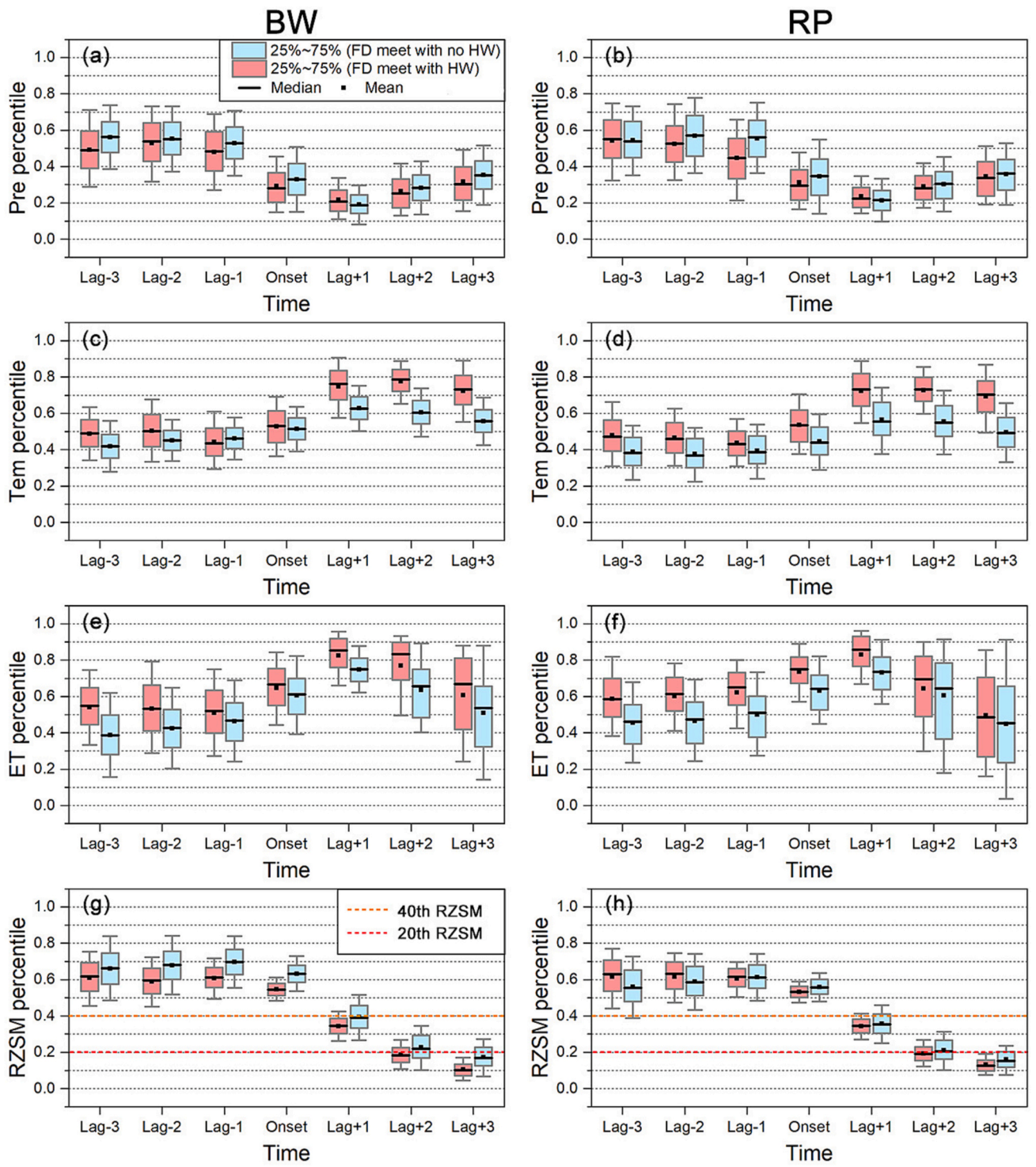

Fig. 11. Percentile changes in the hydro-meteorological variables (precipitation (Pre), Temperature (Tem), Evapotranspiration (ET), and root zone soil moisture (RZSM)) of the two types of flash drought events (i.e., a flash drought (FD) meets with or without a heat wave (HW) event) in adjacent pentads of flash drought onset. "Lag–1" denotes 1 pentad prior to the onset time, while "Lag+1" denotes 1 pentad after the onset time.

There are some limitations of this study that need to be noted. Any study that uses a hydrological model may have associated uncertainties (Van Loon and Van Lanen, 2013; Wang et al., 2020). We note that the validations and applications of the TRAIN model in many previous studies have shown that the model is reliable for simulating ET and RZSM. For example, Stork and Menzel (2016) selected an observation site located in the Upper Rhine Valley near the BW state to validate TRAIN simulated ET and RZSM. The validation results showed that TRAIN simulated the dynamics and range of the daily ET values reasonably well from April to July 2014; the correlation coefficient (*CC*) and Nash efficiency (*NS*) were 0.87 and 0.83, respectively. Meanwhile, the TRAIN model generated very good RZSM dynamics on a daily timescale ($CC = 0.96$ and $NS = 0.91$). In addition to the station-scale validation, Tijdeman and Menzel (2021) selected 60 catchments with near-natural flow across the BW state to validate the TRAIN model from the perspective of water balance. The validation results showed that the

annual average measured runoff for most catchments was in good agreement with the sum of the annual average simulated percolation and surface runoff. These results suggest that there is no systematic bias between the actual and simulated RZSM. Furthermore, in this study, we selected three datasets based on remote sensing, reanalysis, and fusion technology, i.e., the SMAP-L4, ERA5-Land, and GLEAM datasets, to evaluate TRAIN performance. In most areas (80 % of the area across the BW and RP states), the simulated RZSM (ET) had a high correlation (CC $>$ 0.7) with the three (two) datasets. Therefore, these validation studies provide confidences in performing drought identification using the simulated RZSM from the TRAIN model.

Apart from uncertainties, the land-atmosphere feedback mechanism between soil flash drought and heat waves needs to be investigated in future studies (Miralles et al., 2019; Benson and Dirmeyer, 2021; Osman et al., 2022). During a heat wave event, increased ET due to a high atmospheric water vapour pressure difference or radiation can deplete the soil moisture deficit, leading to flash drought (Seneviratne et al., 2010). In contrast, flash droughts affect many processes associated with temperature anomalies (e.g., heat transport between the atmosphere and surface), thus causing or even amplifying heat wave events (Schumacher et al., 2022). From the above mutual feedback perspective, heat waves may be both a driver and a response to flash droughts (Miralles et al., 2019). More importantly, compound flash drought and heat wave events are closely linked to atmospheric circulation anomalies (Zhang et al., 2023b), such as the El Niño-Southern Oscillation (ENSO) and the Arctic Oscillation (AO). Therefore, it is worth to further explore the interaction between flash droughts and heat waves from a perspective of meteorological systematics (Tabari and Willems, 2023), so as to provide technical support for risk analysis and early warning of compound flash drought and heat wave events.

6. Conclusions

In this study, we firstly applied a physically based hydrological model, i.e., the TRAIN model, to simulate the RZSM and ET with daily time steps and on a 1 $\times$ 1 km resolution. Three datasets, ERA5-Land, GLEAM, and SMAP-L4, were selected to evaluate the TRAIN simulated RZSM and ET from 1961 to 2016. Secondly, heat waves and flash drought events were identified based on the daily maximum temperature and TRAIN simulated RZSM. Thereafter, the spatial and temporal distributions of the number of flash droughts, heat waves, and the coincidence of these two events were analysed. Finally, we divided the flash drought events into two types (the first type was a flash drought that occurs with no heat wave while the second type was the opposite) and then compared the drought characteristics (e.g., drought duration and onset speed) of the two types of flash droughts and changes in the hydro-meteorological variables (e.g., precipitation, ET, temperature, and RZSM) associated with the flash drought processes to reveal how heat waves alter flash droughts.

The states of BW and RP in southern Germany were selected as study areas to evaluate the above procedures. The simulated RZSM had the highest correlation with the ERA5-Land products, followed by SMAP-L4 and GLEAM, with regional average correlation coefficients (CC) of 0.765, 0.762, and 0.746, respectively. The CC of the TRAIN simulated ET with ERA5-Land and GLEAM ET were 0.828 and 0.803, respectively. The results of the trend analyses showed a significant increasing trend (p $<$ 0.05) in the number of flash droughts and heat waves in both the BW and RP states. In addition, comparative analysis revealed that the mean duration and onset speed (decline rate) of flash droughts without meeting with heat waves were 10.42 (10.67) pentads and 19.69 (17.16th percentile/pentad) for BW (RP), respectively, while those associated with heat waves were 8.95 (9.53) pentads and 21.77th percentile/pentad (19.91th percentile/pentad) for BW (RP), respectively. These results indicate that flash droughts under the influence of heat waves are generally shorter in duration but faster in occurrence. The findings of this study are helpful for improving our understanding of flash drought processes under the impact of heat waves.

CRediT authorship contribution statement

Menghao Wang: Conceptualization, Methodology, Software, Writing.
Lucas Menzel: Data, Model simulation, Writing-Review & Editing.
Shanhu Jiang: Conceptualization, Project administration.
Liliang Ren: Funding acquisition.
Chong-Yu Xu: Writing-Review & Editing.
Hao Cui: Methodology.

Declaration of competing interest

The authors declare that they have no known competing financial interests or personal relationships that could have appeared to influence the work reported in this paper.

Data availability

Data will be made available on request.

Acknowledgments

This work was financially supported by the State Office for Environment Rhineland-Palatinate, Heidelberg University; the National Natural Science Foundation of China (51979069); the Postgraduate Research & Practice Innovation Program of Jiangsu Province (KYCX21_0503); the Fundamental Research Funds for the Central Universities (B220203037); and the Funds for the China Scholarship Council (202106710042). We acknowledge Leonard Kölsch-Kurtz at University of Heidelberg for his assistance with the TRAIN model simulations.

References

AghaKouchak, A., Farahmand, A., Melton, F.S., Teixeira, J., Anderson, M.C., Wardlow, B. D., Hain, C.R., 2015. Remote sensing of drought: progress, challenges and opportunities. Rev. Geophys. https://doi.org/10.1002/2014RG000456.

AghaKouchak, A., Mirchi, A., Madani, K., Di Baldassarre, G., Nazemi, A., Alborzi, A., Anjileli, H., Azarderakhsh, M., Chiang, F., Hassanzadeh, E., Huning, L.S., Mallakpour, I., Martinez, A., Mazdiyasni, O., Moftakhari, H., Norouzi, H., Sadegh, M., Sadeqi, D., Van Loon, A.F., Wanders, N., 2021. Anthropogenic drought: definition, challenges, and opportunities. Rev. Geophys. https://doi.org/10.1029/2019RG000683.

Albergel, C., Dorigo, W., Reichle, R.H., Balsamo, G., Derosnay, P., Muñoz-sabater, J., Isaksen, L., Dejeu, R., Wagner, W., 2013. Skill and global trend analysis of soil moisture from reanalyses and microwave remote sensing. J. Hydrometeorol. 14, 1259–1277. https://doi.org/10.1175/JHM-D-12-0161.1.

Almendra-Martín, L., Martínez-Fernández, J., Piles, M., González-Zamora, Á., 2021. Comparison of gap-filling techniques applied to the CCI soil moisture database in Southern Europe. Remote Sens. Environ. 258 https://doi.org/10.1016/j.rse.2021.112377.

Almendra-Martín, L., Martínez-Fernández, J., Piles, M., González-Zamora, Á., Benito-Verdugo, P., Gaona, J., 2022. Analysis of soil moisture trends in Europe using rank-based and empirical decomposition approaches. Glob. Planet. Chang. 215 https://doi.org/10.1016/j.gloplacha.2022.103868.

Babaeian, E., Sadeghi, M., Jones, S.B., Montzka, C., Vereecken, H., Tuller, M., 2019. Ground, proximal, and satellite remote sensing of soil moisture. Rev. Geophys. https://doi.org/10.1029/2018RG000618.

Benson, D.O., Dirmeyer, P.A., 2021. Characterizing the relationship between temperature and soil moisture extremes and their role in the exacerbation of heat waves over the contiguous United States. J. Clim. 34, 2175–2187. https://doi.org/10.1175/JCLI-D-20-0440.1.

Bergström, S., 1995. The HBV model. In: Singh, V.P. (Ed.), Computer Models of Watershed Hydrology. Water Resources Publications, Highland Ranch, Colorado, USA, pp. 443–476.

Chen, F., Crow, W.T., Bindlish, R., Colliander, A., Burgin, M.S., Asanuma, J., Aida, K., 2018. Global-scale evaluation of SMAP, SMOS and ASCAT soil moisture products using triple collocation. Remote Sens. Environ. 214, 1–13. https://doi.org/10.1016/j.rse.2018.05.008.

Coumou, D., Lehmann, J., Beckmann, J., 2015. The weakening summer hemisphere mid-latitudes. Science 348 (6232), 324–327. https://doi.org/10.1126/science.1261768.

Dong, C., Menzel, L., 2016. Improving the accuracy of MODIS 8-day snow products with in situ temperature and precipitation data. J. Hydrol. 534, 466–477. https://doi.org/10.1016/j.jhydrol.2015.12.065.
Draper, C.S., Reichle, R.H., De Lannoy, G.J.M., Liu, Q., 2012. Assimilation of passive and active microwave soil moisture retrievals. Geophys. Res. Lett. 39 https://doi.org/10.1029/2011GL050655.
Dumedah, G., Walker, J.P., Merlin, O., 2015. Root-zone soil moisture estimation from assimilation of downscaled soil moisture and ocean salinity data. Adv. Water Resour. 84, 14–22. https://doi.org/10.1016/j.advwatres.2015.07.021.
Edris, S.G., Basara, J.B., Christian, J.I., Hunt, E.D., Otkin, J.A., Salesky, S.T., Illston, B.G., 2023. Analysis of the critical components of flash drought using the standardized evaporative stress ratio. Agric. For. Meteorol. 330, 109288 https://doi.org/10.1016/j.agrformet.2022.109288.
Feng, H., Zhang, M., 2015. Global land moisture trends: drier in dry and wetter in wet over land. Sci. Rep. 5, 1–6. https://doi.org/10.1038/srep18018.
Hao, Z., Hao, F., Xia, Y., Feng, S., Sun, C., Zhang, X., Fu, Y., Hao, Y., Zhang, Y., Meng, Y., 2022. Compound droughts and hot extremes: characteristics, drivers, changes, and impacts. Earth Sci. Rev. https://doi.org/10.1016/j.earscirev.2022.104241.
Hartmann, C., Moser-Reischl, A., Rahman, M.A., Franceschi, E., von Strachwitz, M., Pauleit, S., Pretzsch, H., Rötzer, T., Paeth, H., 2023. The footprint of heat waves and dry spells in the urban climate of Würzburg, Germany, deduced from a continuous measurement campaign during the anomalously warm years 2018–2020. Meteorol. Z. https://doi.org/10.1127/metz/2023/1151.
Hellebrand, H., Van Den Bos, R., Hoffmann, L., Juilleret, J., Krein, A., Pfister, L., 2009. Spatio-temporal variability of behavioral patterns in hydrology in meso-scale basins of the Rhineland Palatinate (1972-2002). Clim. Chang. 93, 223–242. https://doi.org/10.1007/s10584-008-9509-7.
Huang, S., Li, P., Huang, Q., Leng, G., Hou, B., Ma, L., 2017. The propagation from meteorological to hydrological drought and its potential influence factors. J. Hydrol. 547, 184–195. https://doi.org/10.1016/j.jhydrol.2017.01.041.
Ionita, M., Tallaksen, M.L., Kingston, D.G., Stagge, J.H., Laaha, G., Van Lanen, H.A.J., Scholz, P., Chelcea, S.M., Haslinger, K., 2017. The European 2015 drought from a climatological perspective. Hydrol. Earth Syst. Sci. 21, 1397–1419. https://doi.org/10.5194/hess-21-1397-2017.
Jiang, S., Wang, M., Ren, L., Xu, C.Y., Yuan, F., Liu, Y., Lu, Y., Shen, H., 2019. A framework for quantifying the impacts of climate change and human activities on hydrological drought in a semiarid basin of Northern China. Hydrol. Process. 33, 1075–1088. https://doi.org/10.1002/hyp.13386.
Jiang, S., Wei, L., Ren, L., Xu, C.Y., Zhong, F., Wang, M., Zhang, L., Yuan, F., Liu, Y., 2021. Utility of integrated IMERG precipitation and GLEAM potential evapotranspiration products for drought monitoring over mainland China. Atmos. Res. 247 https://doi.org/10.1016/j.atmosres.2020.105141.
Jiang, S., Wang, M., Ren, L., Liu, Y., Zhou, L., Cui, H., Xu, C.Y., 2022. An integrated approach for identification and quantification of ecological drought in rivers from an ecological streamflow perspective. Ecol. Indic. 143 https://doi.org/10.1016/j.ecolind.2022.109410.
Kendall, M.G., 1975. Rank Correlation Methods. Charles Griffin, London.
Li, B., Rodell, M., 2013. Spatial variability and its scale dependency of observed and modeled soil moisture over different climate regions. Hydrol. Earth Syst. Sci. 17, 1177–1188. https://doi.org/10.5194/hess-17-1177-2013.
Lima Alencar, P.H., Paton, E.N., 2022. How do we identify flash droughts? A case study in Central European Croplands. Hydrol. Res. 53, 1150–1165. https://doi.org/10.2166/nh.2022.003.
Liu, Z., Menzel, L., 2016. Identifying long-term variations in vegetation and climatic variables and their scale-dependent relationships: a case study in Southwest Germany. Glob. Planet. Chang. https://doi.org/10.1016/j.gloplacha.2016.10.019.
Liu, Y.I., Zhu, Y.E., Ren, L., Otkin, J., Hunt, E.D., Yang, X., Yuan, F., Jiang, S., 2020a. Two Different Methods for Flash Drought Identification: Comparison of Their Strengths and Limitations. https://doi.org/10.1175/JHM-D-19.
Liu, Y., Zhu, Y., Zhang, L., Ren, L., Yuan, F., Yang, X., Jiang, S., 2020b. Flash droughts characterization over China: from a perspective of the rapid intensification rate. Sci. Total Environ. 704 https://doi.org/10.1016/j.scitotenv.2019.135373.
Mann, H.B., 1945. Nonparametric tests against trend. Econometr. J. Econometr. Soc. 13, 245–259.
Martens, B., Miralles, D.G., Lievens, H., Van Der Schalie, R., De Jeu, R.A.M., Fernández-Prieto, D., Beck, H.E., Dorigo, W.A., Verhoest, N.E.C., 2017. GLEAM v3: satellite-based land evaporation and root-zone soil moisture. Geosci. Model Dev. 10, 1903–1925. https://doi.org/10.5194/gmd-10-1903-2017.
Massey, F.J., 1951. The Kolmogorov-Smirnov test for goodness of fit. J. Am. Stat. Assoc. 46, 68–78. https://doi.org/10.1080/01621459.1951.10500769.
Menzel, L., 1996. Modelling canopy resistances and transpiration of grassland. Phys. Chem. Earth 21, 123–129. https://doi.org/10.1016/S0079-1946(97)85572-3.
Menzel, L., 1997. Modellierung der Evapotranspiration im System Boden-Pflanze-Atmosphäre, Zür. Geogr. Schr. 67 (Institute of Geography, ETH Zürich, Zürich, Switzerland (in German).
Menzel, L., Lang, H., Rohmann, M., 1999. Mean annual actual evaporation. In: Hydrological Atlas of Switzerland, Plate 4.1. https://hydrologicalatlas.ch/products/printed-issue/evaporation/plate-4-1.
Menzel, L., Koch, J., Onigkeit, J., Schaldach, R., 2009. Modelling the effects of land-use and land-cover change on water availability in the Jordan River region. Adv. Geosci. 21, 73–80. https://doi.org/10.5194/adgeo-21-73-2009.
Miralles, D.G., Holmes, T.R.H., De Jeu, R.A.M., Gash, J.H., Meesters, A.G.C.A., Dolman, A.J., 2011. Global land-surface evaporation estimated from satellite-based observations. Hydrol. Earth Syst. Sci. 15, 453–469. https://doi.org/10.5194/hess-15-453-2011.
Miralles, D.G., Gentine, P., Seneviratne, S.I., Teuling, A.J., 2019. Land–atmospheric feedbacks during droughts and heatwaves: state of the science and current challenges. Ann. N. Y. Acad. Sci. 1436, 19–35. https://doi.org/10.1111/nyas.13912.
Mishra, A.K., Singh, V.P., 2010. A review of drought concepts. J. Hydrol. https://doi.org/10.1016/j.jhydrol.2010.07.012.
Mo, K.C., Lettenmaier, D.P., 2015. Heat wave flash droughts in decline. Geophys. Res. Lett. 42, 2823–2829. https://doi.org/10.1002/2015GL064018.
Mo, K.C., Lettenmaier, D.P., 2016. Precipitation deficit flash droughts over the United States. J. Hydrometeorol. 17, 1169–1184. https://doi.org/10.1175/JHM-D-15-0158.1.
Mukherjee, S., Mishra, A.K., Zscheischler, J., Entekhabi, D., 2023. Interaction between dry and hot extremes at a global scale using a cascade modeling framework. Nat. Commun. 14, 1–15. https://doi.org/10.1038/s41467-022-35748-7.
Muñoz-Sabater, J., Dutra, E., Agustí-Panareda, A., Albergel, C., Arduini, G., Balsamo, G., Boussetta, S., Choulga, M., Harrigan, S., Hersbach, H., Martens, B., Miralles, D.G., Piles, M., Rodríguez-Fernández, N.J., Zsoter, E., Buontempo, C., Thépaut, J.N., 2021. ERA5-land: a state-of-the-art global reanalysis dataset for land applications. Earth Syst. Sci. Data 13, 4349–4383. https://doi.org/10.5194/essd-13-4349-2021.
Nguyen, H., Wheeler, M.C., Otkin, J.A., Cowan, T., Frost, A., Stone, R., 2019. Using the evaporative stress index to monitor flash drought in Australia. Environ. Res. Lett. 14 https://doi.org/10.1088/1748-9326/ab2103.
Osman, M., Zaitchik, B.F., Winstead, N.S., 2022. Cascading drought-heat dynamics during the 2021 southwest United States heatwave. Geophys. Res. Lett. 49 https://doi.org/10.1029/2022GL099265.
Otkin, J.A., Anderson, M.C., Hain, C., Svoboda, M., Johnson, D., Mueller, R., Tadesse, T., Wardlow, B., Brown, J., 2016. Assessing the evolution of soil moisture and vegetation conditions during the 2012 United States flash drought. Agric. For. Meteorol. 218–219, 230–242. https://doi.org/10.1016/j.agrformet.2015.12.065.
Otkin, J.A., Svoboda, M., Hunt, E.D., Ford, T.W., Anderson, M.C., Hain, C., Basara, J.B., 2018. Flash droughts: a review and assessment of the challenges imposed by rapid-onset droughts in the United States. Bull. Am. Meteorol. Soc. https://doi.org/10.1175/BAMS-D-17-0149.1.
Pendergrass, A.G., Meehl, G.A., Pulwarty, R., Hobbins, M., Hoell, A., AghaKouchak, A., Bonfils, C.J.W., Gallant, A.J.E., Hoerling, M., Hoffmann, D., Kaatz, L., Lehner, F., Llewellyn, D., Mote, P., Neale, R.B., Overpeck, J.T., Sheffield, A., Stahl, K., Svoboda, M., Wheeler, M.C., Wood, A.W., Woodhouse, C.A., 2020. Flash droughts present a new challenge for subseasonal-to-seasonal prediction. Nat. Clim. Chang. 10, 191–199. https://doi.org/10.1038/s41558-020-0709-0.
Peng, J., Loew, A., Merlin, O., Verhoest, N.E.C., 2017. A review of spatial downscaling of satellite remotely sensed soil moisture. Rev. Geophys. 55, 341–366. https://doi.org/10.1002/2016RG000543.
Perkins, S.E., 2015. A review on the scientific understanding of heatwaves-their measurement, driving mechanisms, and changes at the global scale. Atmos. Res. https://doi.org/10.1016/j.atmosres.2015.05.014.
Peters, W., Krol, M.C., van der Werf, G.R., Houweling, S., Jones, C.D., Hughes, J., Schaefer, K., Masarie, K.A., Jacobson, A.R., Miller, J.B., Cho, C.H., Ramonet, M., Schmidt, M., Ciattaglia, L., Apadula, F., Heltai, D., Meinhardt, F., di Sarra, A.G., Piacentino, S., Sferlazzo, D., Aalto, T., Hatakka, J., Ström, J., Haszpra, L., Meijer, H. A.J., van Der Laan, S., Neubert, R.E.M., Jordan, A., Rodó, X., Morguí, J.A., Vermeulen, A.T., Popa, E., Rozanski, K., Zimnoch, M., Manning, A.C., Leuenberger, M., Uglietti, C., Dolman, A.J., Ciais, P., Heimann, M., Tans, P., 2010. Seven years of recent European net terrestrial carbon dioxide exchange constrained by atmospheric observations. Glob. Chang. Biol. 16, 1317–1337. https://doi.org/10.1111/j.1365-2486.2009.02078.x.
Piles, M., Ballabrera-Poy, J., Muñoz-Sabater, J., 2019. Dominant features of global surface soil moisture variability observed by the SMOS satellite. Remote Sens. 11, 1–21. https://doi.org/10.3390/rs11010095.
Preimesberger, W., Scanlon, T., Su, C.H., Gruber, A., Dorigo, W., 2021. Homogenization of structural breaks in the global ESA CCI soil moisture multisatellite climate data record. IEEE Trans. Geosci. Remote Sens. 59, 2845–2862. https://doi.org/10.1109/TGRS.2020.3012896.
Qing, Y., Wang, S., Ancell, B.C., Yang, Z.L., 2022. Accelerating flash droughts induced by the joint influence of soil moisture depletion and atmospheric aridity. Nat. Commun. 13, 1–10. https://doi.org/10.1038/s41467-022-28752-4.
Rouges, E., Ferranti, L., Kantz, H., Pappenberger, F., 2023. European heatwaves: link to large-scale circulation patterns and intraseasonal drivers. Int. J. Climatol. 1–21 https://doi.org/10.1002/joc.8024.
Schoetter, R., Cattiaux, J., Douville, H., 2015. Changes of western European heat wave characteristics projected by the CMIP5 ensemble. Clim. Dyn. 45, 1601–1616. https://doi.org/10.1007/s00382-014-2434-8.
Schumacher, D.L., Keune, J., Dirmeyer, P., Miralles, D.G., 2022. Drought self-propagation in drylands due to land–atmosphere feedbacks. Nat. Geosci. 15, 262–268. https://doi.org/10.1038/s41561-022-00912-7.
Seneviratne, S.I., Corti, T., Davin, E.L., Hirschi, M., Jaeger, E.B., Lehner, I., Orlowsky, B., Teuling, A.J., 2010. Investigating soil moisture-climate interactions in a changing climate: a review. Earth Sci. Rev. https://doi.org/10.1016/j.earscirev.2010.02.004.
Shah, J., Hari, V., Rakovec, O., Markonis, Y., Samaniego, L., Mishra, V., Hanel, M., Hinz, C., Kumar, R., 2022. Increasing footprint of climate warming on flash droughts occurrence in Europe. Environ. Res. Lett. 17 https://doi.org/10.1088/1748-9326/ac6888.
Skrzyńska, M., Twardosz, R., 2022. Long-term changes in the frequency of exceptionally cold and warm months in Europe (1831–2020). Int. J. Climatol. 2023, 2339–2351. https://doi.org/10.1002/joc.7978.
Stork, M., Menzel, L., 2016. Analysis and simulation of the water and energy balance of intense agriculture in the Upper Rhine valley, south-west Germany. Environ. Earth Sci. 75 https://doi.org/10.1007/s12665-016-5980-z.

Svoboda, M., LeComte, D., Hayes, M., Heim, R., Gleason, K., Angel, J., Rippey, B., Tinker, R., Palecki, M., Stooksbury, D., Miskus, D., Stephens, S., 2002. The drought monitor. Bull. Am. Meteorol. Soc. https://doi.org/10.1175/1520-0477(2002)083<1181:TDM>2.3.CO;2.

Tabari, H., Willems, P., 2023. Global risk assessment of compound hot-dry events in the context of future climate change and socioeconomic factors. npj Clim. Atmos. Sci. 6 https://doi.org/10.1038/s41612-023-00401-7.

Tijdeman, E., Menzel, L., 2021. Controls on the development and persistence of soil moisture stress during drought across southwestern Germany. Hydrol. Earth Syst. Sci. 25, 2009–2025. https://doi.org/10.5194/hess-25-2009-2021.

Tijdeman, E., Blauhut, V., Stoelzle, M., Menzel, L., Stahl, K., 2022. Different drought types and the spatial variability in their hazard, impact, and propagation characteristics. Nat. Hazards Earth Syst. Sci. 22, 2099–2116. https://doi.org/10.5194/nhess-22-2099-2022.

Toreti, A., Belward, A., Perez-Dominguez, I., Naumann, G., Luterbacher, J., Cronie, O., Seguini, L., Manfron, G., Lopez-Lozano, R., Baruth, B., van den Berg, M., Dentener, F., Ceglar, A., Chatzopoulos, T., Zampieri, M., 2019. The exceptional 2018 European water seesaw calls for action on adaptation. Earth's Future 7, 652–663. https://doi.org/10.1029/2019EF001170.

Törnros, T., Menzel, L., 2014. Addressing drought conditions under current and future climates in the Jordan River region. Hydrol. Earth Syst. Sci. 18, 305–318. https://doi.org/10.5194/hess-18-305-2014.

Van Loon, A.F., Van Lanen, H.A.J., 2013. Making the distinction between water scarcity and drought using an observation-modeling framework. Water Resour. Res. 49, 1483–1502. https://doi.org/10.1002/wrcr.20147.

Van Loon, A.F., Gleeson, T., Clark, J., Van Dijk, A.I.J.M., Stahl, K., Hannaford, J., Di Baldassarre, G., Teuling, A.J., Tallaksen, L.M., Uijlenhoet, R., Hannah, D.M., Sheffield, J., Svoboda, M., Verbeiren, B., Wagener, T., Rangecroft, S., Wanders, N., Van Lanen, H.A.J., 2016. Drought in the Anthropocene. Nat. Geosci. https://doi.org/10.1038/ngeo2646.

Vautard, R., Gobiet, A., Jacob, D., Belda, M., Colette, A., Déqué, M., Fernández, J., García-Díez, M., Goergen, K., Güttler, I., Halenka, T., Karacostas, T., Katragkou, E., Keuler, K., Kotlarski, S., Mayer, S., van Meijgaard, E., Nikulin, G., Patarčić, M., Scinocca, J., Sobolowski, S., Suklitsch, M., Teichmann, C., Warrach-Sagi, K., Wulfmeyer, V., Yiou, P., 2013. The simulation of European heat waves from an ensemble of regional climate models within the EURO-CORDEX project. Clim. Dyn. 41, 2555–2575. https://doi.org/10.1007/s00382-013-1714-z.

Wang, Y., Yuan, X., 2022. Land-atmosphere coupling speeds up flash drought onset. Sci. Total Environ. 851, 158109 https://doi.org/10.1016/j.scitotenv.2022.158109.

Wang, M., Jiang, S., Ren, L., Xu, C.Y., Yuan, F., Liu, Y., Yang, X., 2020. An approach for identification and quantification of hydrological drought termination characteristics of natural and human-influenced series. J. Hydrol. 590 https://doi.org/10.1016/j.jhydrol.2020.125384.

Wang, M., Jiang, S., Ren, L., Xu, C.Y., Menzel, L., Yuan, F., Xu, Q., Liu, Y., Yang, X., 2021. Separating the effects of climate change and human activities on drought propagation via a natural and human-impacted catchment comparison method. J. Hydrol. 603 https://doi.org/10.1016/j.jhydrol.2021.126913.

Wang, M., Jiang, S., Ren, L., Xu, C.Y., Wei, L., Cui, H., Yuan, F., Liu, Y., Yang, X., 2022. The development of a nonstationary standardised streamflow index using climate and reservoir indices as covariates. Water Resour. Manag. 36, 1377–1392. https://doi.org/10.1007/s11269-022-03088-2.

Ward, P.J., Daniell, J., Duncan, M., Dunne, A., Hananel, C., Hochrainer-Stigler, S., Tijssen, A., Torresan, S., Ciurean, R., Gill, J.C., Sillmann, J., Couasnon, A., Koks, E., Padrón-Fumero, N., Tatman, S., Tronstad Lund, M., Adesiyun, A., Aerts, J.C.J.H., Alabaster, A., Bulder, B., Campillo Torres, C., Critto, A., Hernández-Martín, R., MacHado, M., Mysiak, J., Orth, R., Palomino Antolín, I., Petrescu, E.C., Reichstein, M., Tiggeloven, T., Van Loon, A.F., Vuong Pham, H., De Ruiter, M.C., 2022. Invited perspectives: a research agenda towards disaster risk management pathways in multi-(hazard-) risk assessment. Nat. Hazards Earth Syst. Sci. 22, 1487–1497. https://doi.org/10.5194/nhess-22-1487-2022.

Yuan, X., Ma, Z., Pan, M., Shi, C., 2015. Microwave remote sensing of short-term droughts during crop growing seasons. Geophys. Res. Lett. 42, 4394–4401. https://doi.org/10.1002/2015GL064125.

Yuan, X., Wang, L., Wu, P., Ji, P., Sheffield, J., Zhang, M., 2019. Anthropogenic shift towards higher risk of flash drought over China. Nat. Commun. 10 https://doi.org/10.1038/s41467-019-12692-7.

Yuan, X., Wang, Y.M., Zhang, M., Wang, L.Y., 2020. A few thoughts on the study of flash drought. Trans. Atmos. Sci. 43 (6), 1086–1095. https://doi.org/10.13878/j.cnki.dqkxxb.20200914002 (in Chinese).

Zhang, F., Zhang, L.W., Shi, J.J., Huang, J.F., 2014. Soil moisture monitoring based on land surface temperature-vegetation index space derived from MODIS data. Pedosphere 24, 450–460. https://doi.org/10.1016/S1002-0160(14)60031-X.

Zhang, L., Liu, Y., Ren, L., Teuling, A.J., Zhu, Y., Wei, L., Zhang, Linyan, Jiang, S., Yang, X., Fang, X., Yin, H., 2022. Analysis of flash droughts in China using machine learning. Hydrol. Earth Syst. Sci. 26, 3241–3261. https://doi.org/10.5194/hess-26-3241-2022.

Zhang, X., Liu, Y., Zhu, Y., Ma, Q., Philippe, G., Qu, Y., Yin, H., 2023a. Probabilistic analysis on the influences of heatwaves during the onset of flash droughts over China. Hydrol. Res. 54, 869–884. https://doi.org/10.2166/nh.2023.022.

Zhang, Y., Hao, Z., Feng, S., Zhang, X., Hao, F., 2023b. Changed relationship between compound dry-hot events and ENSO at the global scale. J. Hydrol. 621, 129559 https://doi.org/10.1016/j.jhydrol.2023.129559.

Zou, L., Xia, J., She, D., 2018. Analysis of impacts of climate change and human activities on hydrological drought: a case study in the Wei River basin, China. Water Resour. Manag. 32, 1421–1438. https://doi.org/10.1007/s11269-017-1877-1.